A selective and orally bioavailable VHL-recruiting PROTAC achieves SMARCA2 degradation *in vivo*

Christiane Kofink[#1], Nicole Trainor[#2§], Barbara Mair[#1], Simon Wöhrle[1], Melanie Wurm[1], Nikolai Mischerikow[1], Michael Roy[2], Gerd Bader[1], Peter Greb[1], Géraldine Garavel[1], Emelyne Diers[2], Ross McLennan[2], Claire Whitworth[2], Vesna Vetma[2], Klaus Rumpel[1], Maximilian Scharnweber[1], Julian E. Fuchs[1], Thomas Gerstberger[1], Yunhai Cui[3], Gabriela Gremel[1], Paolo Chetta[1], Stefan Hopf[1], Nicole Budano[1], Joerg Rinnenthal[1], Gerhard Gmaschitz[1], Moriz Mayer[1], Manfred Koegl[1], Alessio Ciulli[2], Harald Weinstabl*[1], William Farnaby*[2]

[1]Boehringer Ingelheim RCV GmbH & Co KG, 1121, Vienna, Austria.
[2]Centre for Targeted Protein Degradation, School of Life Sciences, University of Dundee, Dow Street, Dundee, DD1 5EH, UK.
[3]Boehringer Ingelheim Pharma GmbH & Co KG, 88397 Biberach, Germany

*To whom correspondence should be addressed. E-mail: harald.weinstabl@boehringer-ingelheim.com, w.farnaby@dundee.ac.uk

[#]These authors contributed equally and have mutually agreed to allow re-ordering for use in CVs or similar material.

[§]Present address: ACRF Chemical Biology Division, Walter and Eliza Hall Institute, Parkville Victoria 3052, Australia

Heterobifunctional degrader molecules - also known as proteolysis-targeting chimeras (PROTACs) - target disease-causing proteins for destruction. They function by binding to both an E3 ligase and to the target protein. The induced proximity results in subsequent ubiquitination of the target protein, earmarking it for degradation by the proteasome. In cells, their mode of action enables degraders to achieve levels of target selectivity, breadth of target scope and efficacy not attainable with a classical inhibitor[1,2]. Due principally to the convenience of administration, oral dosing regimens dominate small molecule therapeutic delivery, however the design of orally available degraders is challenging due to their larger size and related physicochemical properties. To date, the clinical translation of orally active degraders has been confined to the use of a single E3 ligase – Cereblon (CRBN), greatly limiting the potential therapeutic scope of PROTACs[3,4]. Here we show for the first time that orally bioavailable PROTACs can be developed that utilise other E3 ligases, in this case the von Hippel-Lindau (VHL)/ElonginB-ElonginC (VCB) complex, which is recruited by a ligand of larger molecular weight than the immunomodulatory drugs (IMiDs) that bind CRBN. We found that design of linker composition and exit vector placement could be guided and rationalised by ternary co-crystal structures, yielding molecules which exhibit high potency and suitable pharmacokinetic properties to translate to oral *in vivo* efficacy. Furthermore, our lead molecule ACBI2 demonstrates strong selectivity for the BAF (SWI/SNF) complex ATPase SMARCA2 over its highly similar paralogue SMARCA4 in human whole blood and consistent preferential degradation of SMARCA2 in all cell lines tested. This permits pharmacological evaluation of the synthetic lethality concept of selectively targeting SMARCA2 in SMARCA4-deficient cancers *in vivo* and *in vitro* [5–7]. We qualify ACBI2 as an orally bioavailable SMARCA2 degrader that will be made freely available to the community. We anticipate that our results and the methodologies employed will provide a blueprint to arrive at oral efficacy of other E3-recruiting degraders.

Discovery of a novel potent SMARCA2/4/PBRM1 binder to enable targeted protein degradation.

PROTACs are often made by the up-cycling of existing protein of interest (POI) binders, allowing quick generation of protein degrader tool compounds. However, the optimisation of physicochemical properties to turn *in vitro* degrader tools into *in vivo* drugs often remains challenging and can prohibit the progression of the compounds into the clinic. For the SMARCA2/4 bromodomains (BDs), two sub-micromolar binders have been described in the literature. PFI-3 was reported as a *bona fide* SMARCA2/4 BD-binding tool compound (Figure **1a**), albeit with modest affinity and a latent risk for unfavourable chemical stability [8]. In addition, Genentech reported a phenol-amino-pyridazine derivative (GEN-1) with attractive stability, physicochemical properties and affinity (Figure **1a**) [9]. We successfully used this motif to generate SMARCA2/4 degraders[10], but the polarity of the binding motif prohibited subsequent optimisation towards sufficient oral bioavailability for this VHL-based PROTAC. Driven by the multiple advantages of orally bioavailable drugs, such as a high patient acceptance, the possibility of non-sterile self-administration, cost-effectiveness and ease of large-scale manufacturing[11], we set out to obtain orally active SMARCA2 degraders.

As a first step, we elected to discover a novel SMARCA2 bromodomain binder, incorporating only the absolute minimum of hydrogen bond donors, a high degree of rigidity and distinct and well-defined exit vectors. In addition, a reliable synthetic route, with the possibility for late-stage functionalisation, was considered essential. Inspired by Sutherell et al. [12], who previously identified binders for the bromodomain (BD) of PBRM1 ($PBRM1^{BD5}$), which shares a high degree of similarity to the bromodomain to SMARCA2, we first characterised the molecular interactions that are mandatory for BD binding using a high-resolution crystal structure of "compound 26" [12](PDB: 5FH7, Figure **1a**). We found the halogen bond to the $Met371^{PBRM1}$ backbone (BB) carbonyl and the hydrogen bonding interaction between $Asn739^{PBRM1}$ and the quinazolinone core to be indispensable. Incorporating insights of halogen bond optimisation from an alternative benzoxazinone lead series (Figure **1b**) to the quinazoline core led to the design of scaffold compound **1** (Figure **1c**). We also evaluated the possibility to replace the halogen bonding interaction by a hydrogen bonding interaction in compound **2**, however this was detrimental to binding affinity (Figure **1c**). Next, we hypothesised that placing a basic centre close to $Glu1417^{SMARCA2}$ could improve the binding affinity and would also balance the solubility of the compound. The attachment of a piperidine was superior to other linear and cyclic basic moieties, such as piperazines or amino-carbocycles, and led us to compound **3** as a novel, purposefully designed SMARCA2/4 BD binding motif for PROTAC generation (Figure **1c**). The expected binding mode of compound **3** was confirmed by solving a co-crystal structure of its nor-methyl analogue compound **4** with $SMARCA2^{BD}$ (Figure **1d**, PDB: tbd, 1.32 Å resolution, see Supplementary Table **1**) revealing that the key interactions of the quinazoline core towards Asn1464 and Leu1456 as well as Glu1417 via the basic nitrogen of the piperidine are addressed in the $SMARCA2^{BD}$. Finally, SPR binding kinetics of compound **3** (SPR $SMARCA2^{BD}K_D$ = 46 nM) revealed a similar behaviour as previously reported for GEN-1 (SPR $SMARCA2^{BD}K_D$ = 206 nM), however with significantly reduced hydrogen bond donor count. (Figure **1e,** Extended Data Table **1**), thus offering a superior starting point for the generation of orally available PROTACs.

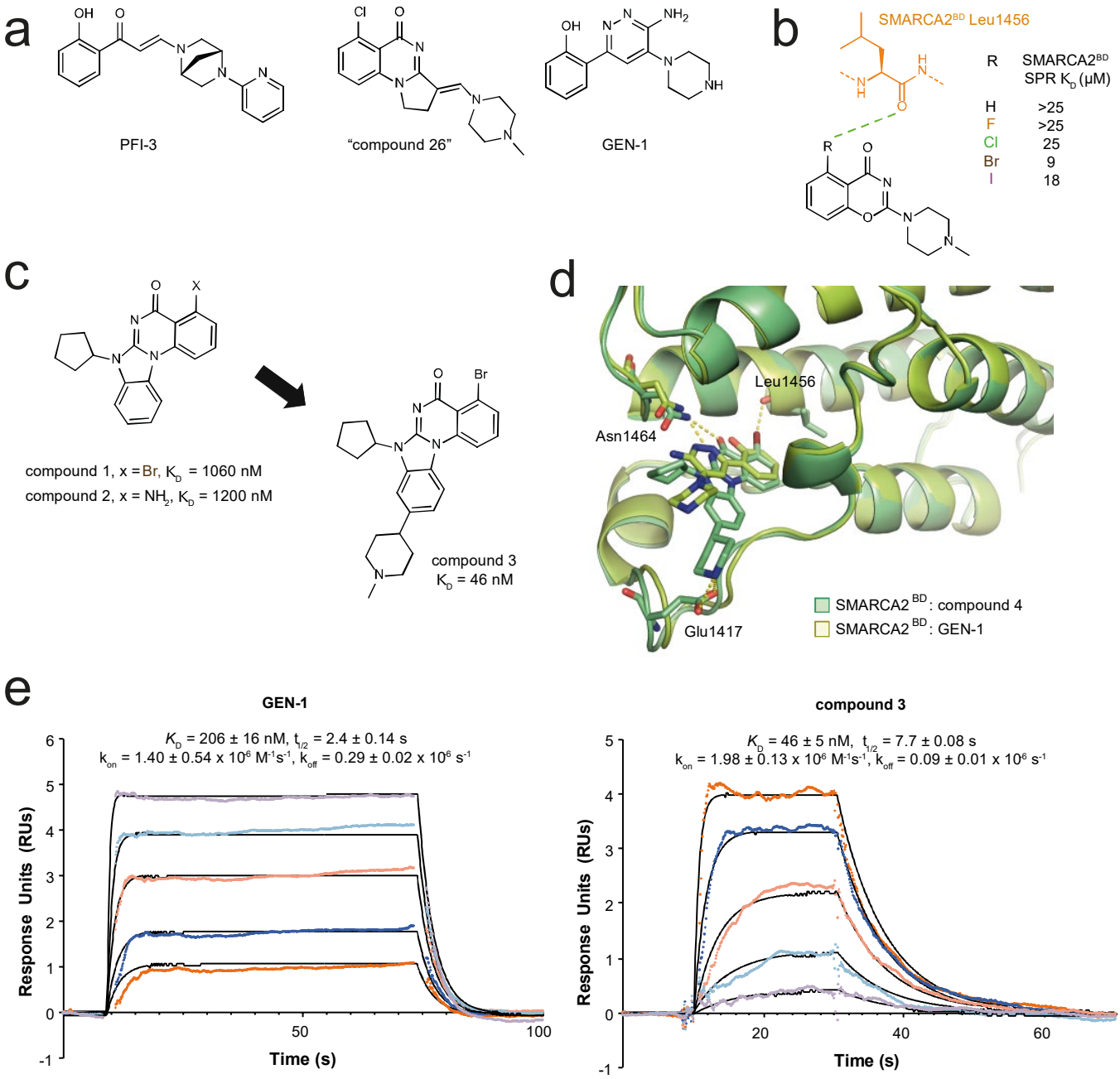

Figure 1. Biophysical and structural characterisation of compound 3 and previously disclosed SMARCA bromodomain binders. a. Comparison of previously disclosed SMARCA binders with sub-μM binding affinity: PFI-3[8], GEN-1[9], "compound-26"[12] . **b.** Optimisation of the halogen bonding interaction to Leu1456 based on an alternative benzoxazinone lead series. **c.** SAR of novel SMARCA binding scaffold with reduced hydrogen bond donor count. **d.** Superposition of the SMARCA2^{BD} : compound **4** complex (green, a close analogue of compound **3**) with PDB: 6HAZ (yellow, GEN-1) highlighting key interactions towards Asn1464, Leu1456 and Glu1417. **e.** SPR sensorgrams for binding of compound **3**/GEN-1 to SMARCA2^{BD}; mean values reported with standard deviation (n=3 independent experiments).

Identification of an *in vivo* active SMARCA2 degrader via exit vector hopping

We previously reported potent dual degraders of SMARCA2/4, utilising a phenolic exit vector from the VHL ligand, and hypothesised that PROTACs based on our new ligand compound **3** would offer new opportunities for *in vivo* degrader optimisation[10]. PROTACs with PEG- and alkyl-based linkers showed moderate target

degradation in RKO cells, with 27 – 75% maximal degradation (D_{max}) for SMARCA2 (Extended Data Table **2**). Notably, compound **5** demonstrated partial degradation of SMARCA2 (DC_{50} = 78 nM, D_{max} = 46%) while sparing SMARCA4 completely (Figure **2a**). Kinetic experiments demonstrated that compound **5** did not show degradation of SMARCA2 at 4 hours, suggesting a slow rate of degradation (Extended Data Table **2**). Rapid degradation kinetics may reduce the need for prolonged *in vivo* exposure. We have previously shown that E3 Ligase : PROTAC : POI ternary complex stability can impact the rate of degradation[13]. To support our understanding of the thermodynamics of ternary complex formation in this series, we established SPR and TR-FRET assays (Extended Data Tables **1 and 3**), and solved a high resolution co-crystal structure of the VCB : compound **5 :** $SMARCA2^{BD}$ complex (PDB: tbd, **Figure 2b**, see Supplementary Table **2**). Consistent with poor target degradation at 4 hours, the data show moderate ternary complex binding affinities and a limited buried surface for this ternary complex (1837 $Å^2$). Whilst the position of $SMARCA2^{BD}$ may be influenced by crystal contacts formed in the closely packed crystal lattice (Extended Data Figure **1a-e**), the structure indicates a *de novo* protein-protein interaction (PPI) between Asn67 of VHL and Gln1469 of SMARCA2. It is noteworthy that SMARCA4 features a leucine residue in this position and is thus less capable of forming such a PPI, offering a possible rationale for the observed selectivity of compound **5**. In pursuit of more stable complexes that could result in rapid degradation based on the co-crystal structure, we switched the VHL exit vector from the phenolic to the benzylic position (Figure **2c**), which was enabled by new synthetic methods (see SI). This resulted in compound **6**, a fast and potent dual degrader of SMARCA2/4 (SMARCA2 DC_{50} = 2 nM, D_{max} = 77% ; SMARCA4 DC_{50} = 5 nM, D_{max} = 86%, in RKO cells after 4 hours) (Figure **2c**, Extended Data Table **3**) that displayed the expected antiproliferative effect (IC_{50} = 2 nM, Extended Data Table **4**) in a SMARCA4 deficient lung cancer cell line, NCI-H1568. We also observed concurrent degradation of PBRM1 and could rescue SMARCA2 degradation by inhibition of the VHL-HIF1-α interaction using VH298, neddylation inhibition using MLN4924 or proteasome inhibition by MG132 (Extended Data Figure **2a-c**). We solved the ternary complex crystal structure of VCB : compound **6 :** $SMARCA2^{BD}$, in which the compound adopts a different binding pose to that of compound **5** with an increased buried surface area of 2050 $Å^2$ (Figure **2d**), consistent with an observed increase in ternary complex half-life and ternary binding affinity in SPR and TR-FRET assays, compared with compound **5**, offering an explanation for the differential cellular SAR (Figure **2a,** Extended Data tables **1 and 3**). PK studies revealed that the improved microsomal stability of compound **6** compared with compounds from the phenolic series (Extended Data Table **4**) translated into a low clearance of 7 mL/min/kg in mouse, and the compound was quantitatively bioavailable upon subcutaneous administration (Extended Data Table **5**). Single dose subcutaneous treatment of an NCI-H1568 tumour xenograft model with compound **6** reduced median SMARCA2 levels in tumours by 82% relative to control-treated samples at six hours after treatment, with slight recovery of the signal observed after 48 hours treatment, to a median decrease of 69% (Figure **2e**). This translated in significant tumour growth inhibition (TGI) in two different treatment regimens that were both well tolerated (Figure **2f,** Extended Data Table **5**). In tumour samples collected at the end of the study, compound **6** treatment resulted in undetectable levels of SMARCA2 as assessed by IHC (Extended Data Figure **2d**). In summary, a structure guided exit-vector hop enabled discovery of small molecule degraders that form higher affinity complexes, enabling demonstration of prolonged biomarker modulation and anti-tumour efficacy *in vivo* in a SMARCA4-deficient xenograft model.

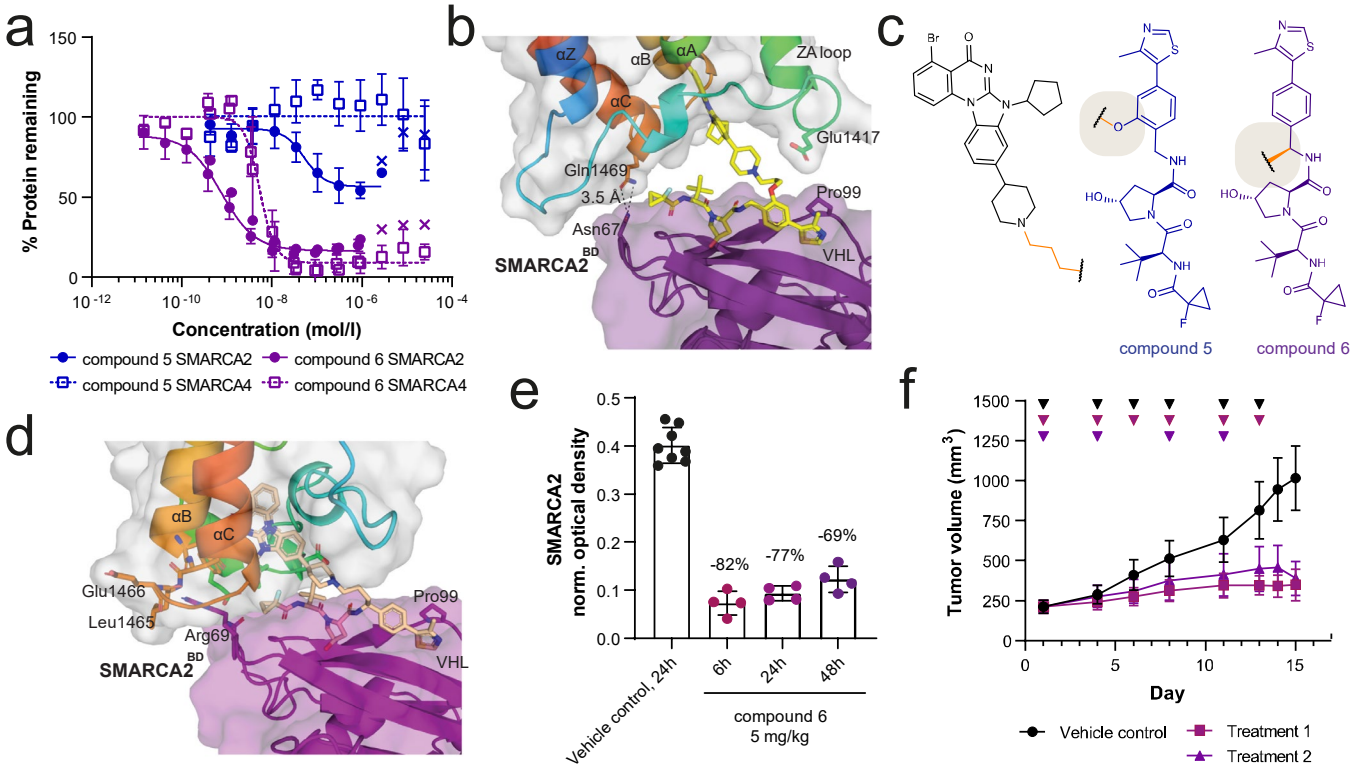

Figure 2. Ternary structure guided design of an *in vivo* active dual SMARCA2/4 degrader: a. Dose response curves for SMARCA2 and SMARCA4 protein levels measured by capillary electrophoresis normalised to DMSO control, following compound treatment of RKO cells for 18 h. Values are the mean of 3-6 independent experiments, error bars indicate standard deviation. Values indicated by x are excluded from curve fit (hook effect). **b.** Ternary X-ray crystal structure for VCB : compound **5** : SMARCA2^{BD}. **c.** Structures of compound **5** and compound **6** highlighting the VHL exit vector switch. **d.** Ternary X-ray crystal structure for VCB : compound **6** : SMARCA2^{BD}. **e.** NCI-H1568 tumour bearing mice (average tumour size ~260 mm^3) were treated subcutaneously with 5 mg/kg compound **6** (n=4 animals per time point) or vehicle control (n=8 animals, 24 h only) and tumours were collected 6, 24 and 48 h after treatment. SMARCA2 levels in viable tumour tissue were determined using DAB-based IHC staining, using background-normalised DAB optical density (OD) within the viable tumour area of an individual tumour. Mean OD levels and standard deviations are indicated. Percentages represent the median levels of SMARCA2 signal decrease relative to vehicle control-treated samples. **f.** NCI-H1568 tumour bearing mice (average tumour size ~210mm^3) were treated subcutaneously with 5 mg/kg compound **6** in two treatment schedules ("Treatment 1/2", see methods for details), resulting in a TGI of 77 and 84%, respectively, at day 15 after the start of treatment (adj. p-value = 0.0002 for either regimen vs. control, U-test with Bonferroni-Holm correction). Values represent the mean of 10 animals per group, error bars indicate standard deviation. Downward triangles indicate days of treatment application.

A structure guided approach to discover selective, orally bioavailable VHL PROTACs

Based on our observations that the short three carbon linker used in compound **6** efficiently forms a high affinity ternary complex leading to potent degradation of SMARCA2/4, we elected to focus on a small set of alkyl and ether based analogues with the objective of improving selectivity and oral bioavailability. Linker elongation and branching led to compounds, such as compound **7** and compound **8**, which show remarkable selectivity for SMARCA2 over SMARCA4 degradation (Extended Data Table **2**; Figure **3a**). Linker branching by installation of an additional methyl group as in compound **8** further improved the permeability in a Caco-2 cell assay (Extended Data Table **4**). To gain a better understanding for the molecular basis of this selectivity, we again turned to crystal

structure analysis. We were able to solve the ternary crystal structure of compound **9**, a close analogue of compound **8**, that only differs in the VHL binder site where the fluorine is replaced by a dimethyl amino group (Figure **3a, 3b**). This ternary structure revealed that an extensive network of *de novo* electrostatic interactions between SMARCA2 and VHL was formed, leading to the formation of a ternary complex significantly different from the previously observed ones (Extended Data Figure **3a**). Furthermore, the SMARCA2-specific residue Gln1469 was involved in VHL : $SMARCA2^{BD}$ interactions, as previously observed for the SMARCA2-selective molecule compound **5**, albeit in this case in the context of a different overall arrangement of the two proteins. In SMARCA2, Gln1469 positively interacts with VHL residues Phe91 and Asp92 via hydrogen bonds, an interaction that cannot occur in SMARCA4 that harbours Leu1545 instead of Gln1469. In summary, linker elongation with an oxygen and linker branching gave rise to compounds that were selective towards SMARCA2, a preference rationalised by ternary complex structures. However, despite good microsomal stability and measurable Caco-2 permeability (Extended Data Table **4**), the compounds showed a high efflux ratio, preventing oral bioavailability.

Learning that linker elongation and branching improves selectivity and permeability, we hypothesised that this should also apply to the more lipophilic all-carbon series. Linker elongation from three to five carbon atoms also resulted in a slight SMARCA2/4 selectivity improvement, by two- to three-fold within the all-carbon linker series, as observed by comparing compound **6** with compound **10** (Extended Data Table **2**). Linker elongation led to an improved permeability for compound **10**, which, due to its good microsomal stability and moderate solubility (Extended Data Table **4**), constituted the first orally bioavailable SMARCA2 VHL PROTAC (Figure **3c,** Extended Data Table **5**). We tested compound **10** in an NCI-H1568 xenograft study, treating mice orally with 100 mg/kg, and evaluated SMARCA2 levels in viable tumour tissue 48 hours after treatment start. A median decrease of 80% compared to vehicle control-treated tumours was detected (Figure **3d**). In subsequent studies, mice were treated orally with 30 mg/kg or 100 mg/kg compound **10** daily. A significant TGI of 64 % within the 30 mg/kg and 76% within the 100 mg/kg treatment group could be reached at day 17 of the experiment (Figure **3e**). The compound was well tolerated in both dose groups as assessed by body weight changes (Extended Data Figure **3b**). At the end of the study, SMARCA2 levels were undetectable by IHC in most treated tumour samples from both groups (Extended Data Figure **3c**). Together, compound **10** achieved significant *in vivo* activity and oral bioavailability, unprecedented for VHL-based PROTACs.

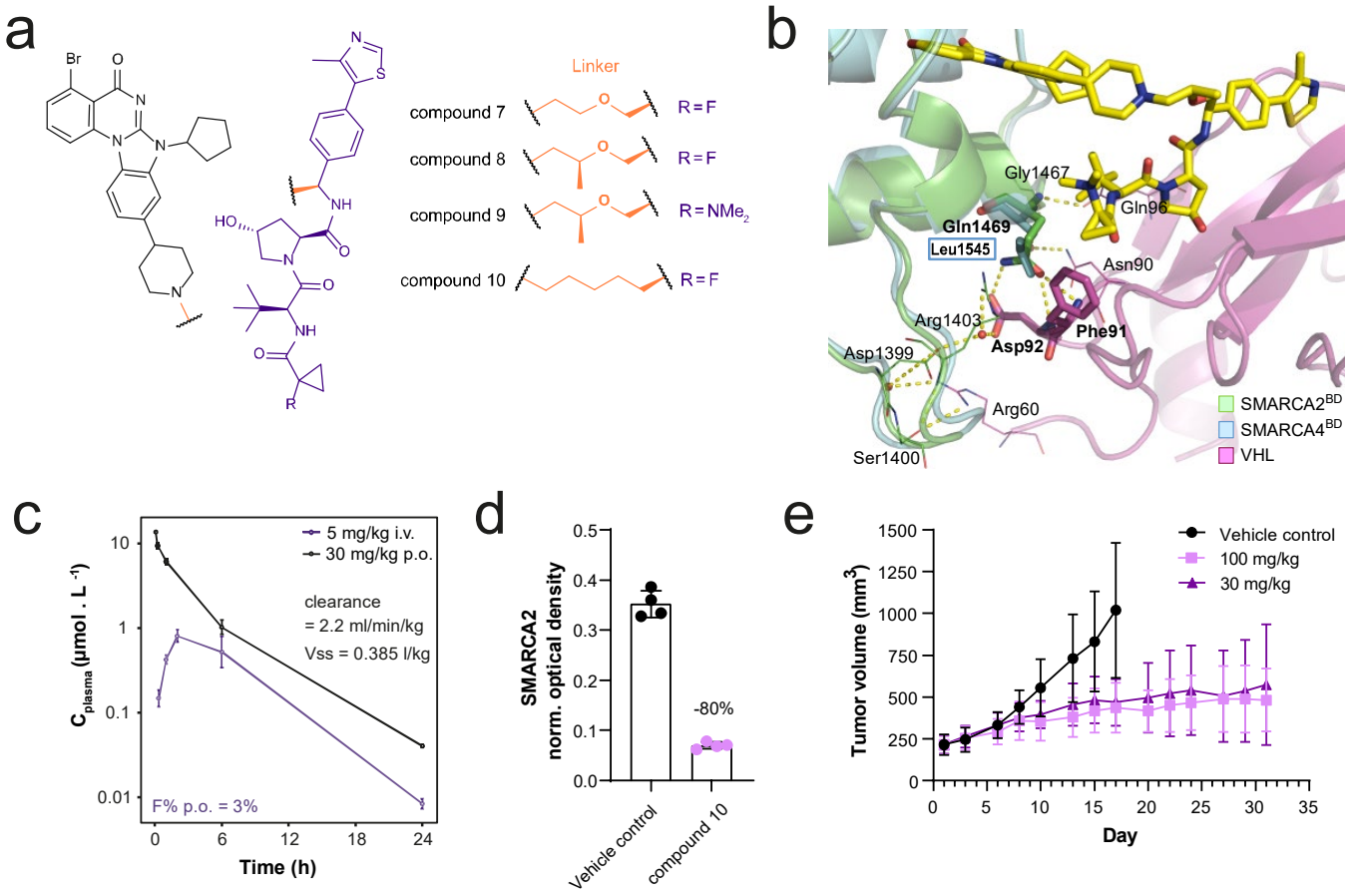

Figure 3. Design and *in vivo* evaluation of an orally bioavailable VHL-based PROTAC. a. Structures of compound **7**, compound **8**, compound **9** and compound **10**. **b.** Co-crystal structure of VCB : compound **9** : SMARCA2^{BD} in ribbon representation. VCB is shown in magenta, SMARCA2^{BD} is shown in green with bound PROTAC shown in sticks with yellow carbons overlayed with SMARCA4^{BD} in ribbon representation shown in blue. Represented are the key PPIs between VCB and SMARCA2^{BD}/SMARCA4^{BD}, highlighting the selectivity-inducing hydrogen bonding between Gln1469 of SMARCA2^{BD} and VCB vs. Leu1545 in SMARCA4^{BD}. **c.** Plasma profiles of compound **10** in mouse after administration of 5 mg/kg i.v. or 30 mg/kg p.o. The oral bioavailability of compound **10** was 3%. **d.** NCI-H1568 tumour bearing mice were treated orally with 100 mg/kg compound **10** or vehicle control (n=4 animals per group) and tumours were collected 48 h after treatment. The average tumour size at treatment start was ~290 mm^3. SMARCA2 levels in viable tumour tissue were determined using DAB-based IHC staining. Each datapoint represents the background-normalised DAB optical density (OD) within the viable tumour area of one tumour section, corresponding to one individual tumour. Mean OD levels and standard deviations are indicated in the graph. Numbers above the data points represent the median levels of SMARCA2 signal decrease relative to vehicle control-treated samples. **e.** NCI-H1568 tumour bearing mice were treated orally with compound **10** at 30 or 100 mg/kg daily. Average tumour volume at the beginning of treatment was ~220 mm^3. At day 17 after treatment start, TGI was 76% for the 100 mg/kg and 64% for the 30 mg/kg treatment group (adj. p-value = 0.0009 for either regimen vs. control, U-test with Bonferroni-Holm correction). Values represent the mean of 10 animals per group, error bars indicate standard deviation.

ACBI2 is an orally active degrader that selectively degrades SMARCA2 over SMARCA4

It has been shown that despite having properties such as molecular weight >1000 Da, 2D topological polar surface area and number of rotatable bonds well beyond those deemed optimal for passive cell permeability,

PROTACs can adopt more compact 3D conformations that yield 3D polar surface and radius of gyration more consistent with that required for permeability[14,15]. To date, this has been translated into oral bioavailability only for CRBN-based PROTACs[16–18] and led to the perception that it is more challenging to achieve for VHL-based degraders[19]. We hypothesised that if we could enable more compact conformations of compound **10** via changes to the linker region, we could enhance absorption, reduce efflux, and ultimately enhance oral bioavailability. We therefore incorporated an additional methyl group on the C5 linker of compound **10**, a change which on the analogous ether series (see compound **7** vs. compound **8**) gave improvements in Caco-2 permeability. This modification yielded ACBI2, a highly potent VHL PROTAC (IC_{50} = 7 nM), which degrades SMARCA2 with a >30-fold window over SMARCA4 in RKO cells (SMARCA2 DC_{50} = 1 nM, SMARCA4 DC_{50} = 32 nM) (Extended Data Table **2**). The branched linker significantly reduced ACBI2 efflux, which directly resulted in an improved oral bioavailability of 22% (Figure **4a**).

Molecular dynamics (MD) simulations and NMR studies comparing compound **10** and ACBI2 were performed to provide a molecular basis for the link between conformational restraint and reduced efflux ratio. Conformational ensembles from simulations indeed showed a trend towards collapsed structures with lower radius of gyration leading to lower free energies for ACBI2. Consequently, lower polar surface area values tended to be favoured within the conformational ensemble of ACBI2 (Extended Data Figure **4a**). NMR studies were carried out to evaluate long-range nuclear Overhauser effects (NOEs) (Figure **4b**). We determined long range NOEs for ACBI2 that were not detectable in compound **10**. Furthermore, under identical experimental conditions, the sign of the NOE crosspeaks was different for the two compounds, indicating a different degree of mobility and therefore compactness of the compounds, with ACBI2 having the more compact structure (see SI Supplementary Figure **1**).

Encouraged by the improved oral bioavailability and selectivity profile of ACBI2, we characterised the compound in more detail *in vitro*. A panel of cell lines showed varying levels of sensitivity to ACBI2, correlating with genetic dependency on SMARCA2 due to mutation or lower expression of SMARCA4 (Figure **4c**). Accordingly, ACBI2 treatment caused rapid and complete degradation of SMARCA2 in two sensitive cell lines (A549 and NCI-H1568; Extended Data Figure **4b**). As for compound **6**, we could rescue SMARCA2 (and PBRM1) degradation by inhibition of VHL, neddylation or the proteasome (Extended Data Figure **4c** and **4d**). We also detected decreased mRNA levels of *KRT80*, a gene that is transcriptionally regulated downstream of SMARCA2 and has been proposed as a biomarker associated with SMARCA2 inhibition[20] (Extended Data Figure **4e**), confirming functional perturbation of BAF complex roles by ACBI2. Unbiased whole cell proteomic analysis demonstrated proteome-wide selectivity for degradation of SMARCA2 and, as expected from the POI binding moiety, PBRM1 in protein lysates prepared from NCI-H1568 cells, similar to compound **6** (Figure 4**d**, Extended Data Figure **4f,** Supplementary File Proteomics). Interestingly, we observed that the extent of selectivity of SMARCA2 degradation over SMARCA4 varied in cell lines expressing both proteins (HCT116 and RKO, Extended Data Figure **5a**). We investigated if this might be correlated with differences in half-life or re-synthesis rates of either SMARCA2 or SMARCA4, and indeed observed a trend towards higher selectivity in RKO, the cell line with shorter half-lives and faster re-synthesis of both SMARCA2 and SMARCA4 (Extended Data Figure **5b and 5c**). We tested ACBI2 selectivity in five additional cell lines and confirmed preferential degradation of SMARCA2 over SMARCA4 in all of them (Extended Data Figure **5d**). We cannot formally rule out other differences between these cell lines as contributors to differential selectivity (e.g. proliferation rate, mutations or expression levels of SMARCA2, SMARCA4 and VHL or ratios thereof), but do not observe obvious trends towards either of those in this small cell line panel.

We went on to test ACBI2 *in vivo* and observed dose-dependent SMARCA2 degradation in NCI-H1568 and A549 engrafted tumour bearing mice following short-term treatment (Figure **4e and 4f**). Correspondingly, ACBI2 (administered at 80 mg/kg orally qd) significantly inhibited tumour growth in an A549 xenograft model (**Figure 4g**) and was well tolerated (Extended Data Figure **5e**). Median SMARCA2 protein levels in tumours collected at the end of this study were decreased by 90% compared to control treated animals (Figure **4h**). Finally, we tested ACBI2 *ex vivo* treatment of human whole blood, obtained from three different healthy donors, and observed near-complete degradation of SMARCA2 with clear selectivity over SMARCA4 (Figure **4i**). Together, these data

demonstrate that oral bioavailability in combination with preferential degradation of one close paralog, SMARCA2, over the other, SMARCA4, can be achieved *in vitro* and *in vivo* with our VHL based protein degrader ACBI2.

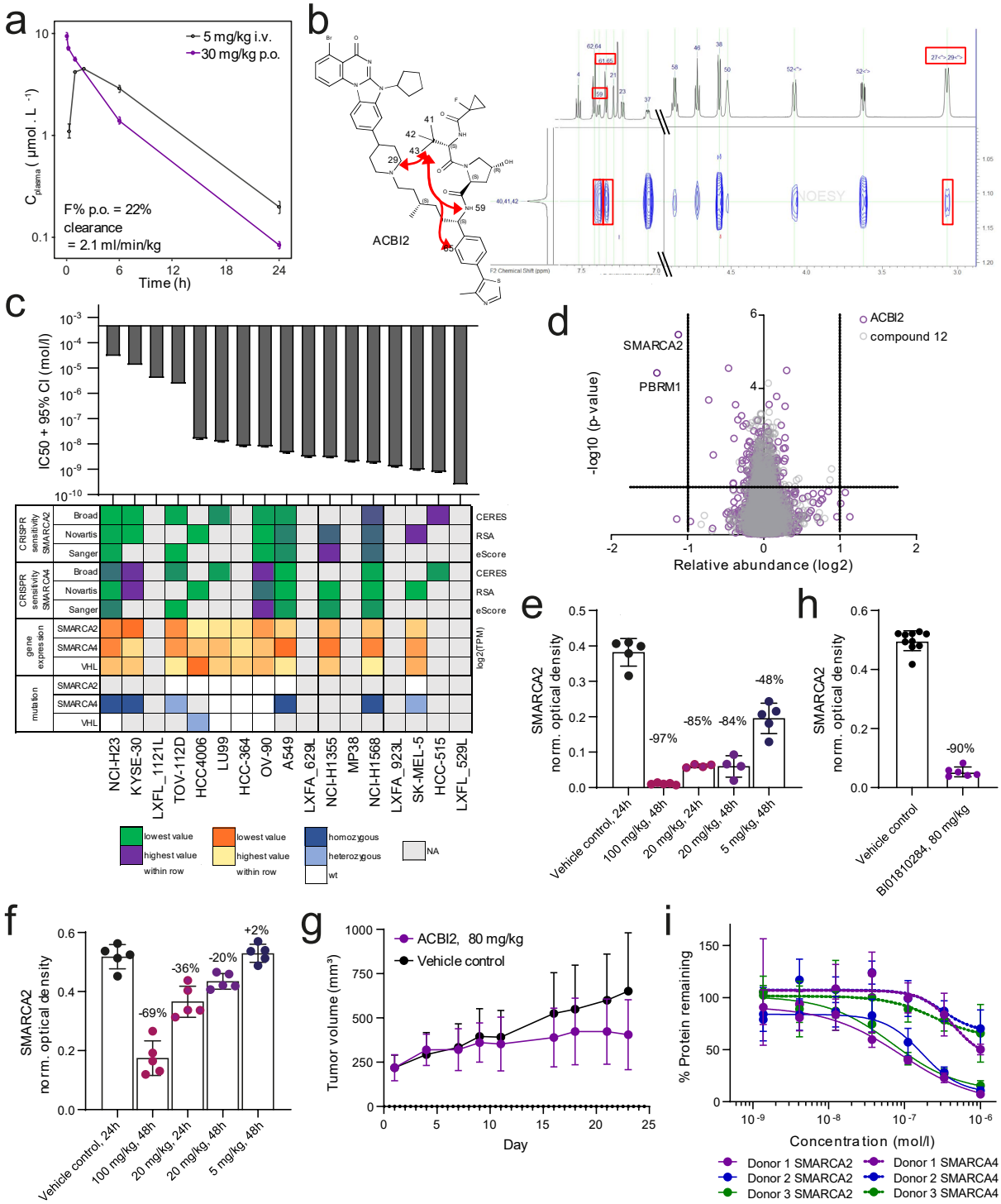

Figure 4. ACBI2 is an orally bioavailable degrader that preferentially degrades SMARCA2 and induces lung cancer tumour growth inhibition. a. Plasma profiles of ACBI2 in mouse after administration of 5 mg/kg i.v. or 30 mg/kg p.o. The oral bioavailability of ACBI2 was 22%. **b.** Structure of ACBI2 and selected long range NOEs are highlighted in the strip plot of the 2D NOESY spectra. **c.** The indicated cell lines were treated with ACBI2 for 144-192 h, and

cell viability was measured using CellTiter Glo (n= 2-7 independent experiments). Displayed are IC_{50} values with 95% confidence interval from 4-parametric logistic curve fit. Heatmap provides sensitivity to genetic depletion by CRISPR, gene expression and mutation data from DepMap/CCLE, scaled for each row, i. e. across cell lines, but separate for each parameter. **d.** Effects of ACBI2 (purple) and negative control compound **12** (gray, *cis*-hydroxyproline analogue of ACBI2 which is not capable of binding VHL) on the proteome of NCI-H1568 cells treated with the compounds at 100 nM for 4 h. Data are plotted as the $\log_2$ of the normalised fold change in abundance against $-\log_{10}$ of the p-value per protein from 3 independent experiments. All *t*-tests performed were two-tailed assuming equal variances. **e.** NCI-H1568 (average tumour size at treatment start ~470 mm^3) or **f.** A549 (average tumour size at treatment start ~360 mm^3) tumour bearing mice were treated orally with 100 mg/kg, 20 mg/kg, 5mg/kg ACBI2 or vehicle control (n=5 animals per group) and tumours collected 24 or 48 h after treatment. Tumours from one NCI-H1568 tumour-carrying animal treated with 20 mg/kg ACBI2 and collected at 24 and 48 h, respectively, could not be analysed due to poor tumour quality. SMARCA2 levels in viable tumour tissue were determined using DAB-based IHC staining. Each datapoint represents the background-normalised DAB optical density (OD) within the viable tumour area of one tumour section, corresponding to an individual tumour. Mean OD levels and standard deviations are indicated in the graphs. Numbers above the datapoints represent median levels of SMARCA2 signal decrease relative to control-treated samples. **g.** A549 tumour bearing mice were treated orally with 80 mg/kg ACBI2 once daily. Average tumour volume at the start of treatment were ~220 mm^3. At day 21 of treatment, a TGI of 47% (p-value = 0.0351 vs. control) was measured. Values represent the mean of 10 animals per group, error bars indicate standard deviation. **h.** At the end of the study shown in **g**, tumours were collected and SMARCA2 levels in viable tumour tissue determined using DAB-based IHC staining (as for **e** and **f**). The median level of SMARCA2 staining in ACBI2 treated tumours was reduced by 90% compared to vehicle control-treated tumours. **i.** Human whole blood from three healthy donors was treated with the indicated concentrations of ACBI2 for 18 h in the dark. Protein was extracted from PBMCs and relative SMARCA2 and SMARCA4 levels (each normalised to GAPDH) measured using automated Western blotting. Each data point represents an average value based on three biological replicates, shown as a percentage relative to DMSO-treated control samples. Error bars indicate standard deviation.

Discussion

An oral route of administration for a new small molecule therapeutic is currently considered the rule rather than the exception. Despite an increasing number of orally dosed bifunctional degraders in the clinic, all those disclosed to date rely solely on ImiDs to recruit the CRBN E3 ligase recognition subunit [16–18]. Whilst successful, this restriction greatly limits the long-term therapeutic scope and is predicated to some degree on an assumption that larger E3 ligase recruiting motifs cannot yield orally available PROTACs. Here, we introduce three principles for arriving at orally available VHL-based degraders that we believe to be of general utility: Firstly, the *de novo* design of novel and potent protein of interest binders that display improved physicochemical properties at the outset of bifunctional degrader design. Secondly, crystallographic knowledge of ternary complex binding modes guides exploration of new exit vector space to achieve more stable complexes and consequently more potent and faster degraders. Lastly, we show how small linker modifications can influence compound conformations leading to more compact arrangements with reduced 3D polar surface area and radius of gyration. We were also able to identify compounds that selectively degrade SMARCA2 over SMARCA4 without appreciable differences in affinity for the binding ligand alone. As has been shown previously in the field of targeted protein degradation[21,22], we were also able to identify compounds that discriminate and preferentially degrade highly homologous target proteins (here, the bromodomains of SMARCA2 over SMARCA4) without appreciable differences in binding affinity for the target ligand alone.

BAF (SWI/SNF) chromatin remodelling complexes play critical roles in cancer[23,24]. For example, it has recently been shown that androgen receptor (AR) and forkhead box A1 (FOXA1) expressing prostate cancer cells

are sensitive to simultaneous degradation of BAF complex subunits SMARCA2, SMARCA4 and PBRM1[25]. The synthetic lethality between SMARCA2 and SMARCA4, resulting in sensitivity of SMARCA4-deficient cells to loss of SMARCA2, has been discovered and validated by genetic methods [5–7], but pharmacological validation and exploitation of this synthetic lethal relationship has been hampered by the lack of suitably selective small molecules, in particular for effective *in vivo* use in animal models[10,20]. Here we show that ACBI2 is capable of inducing near-complete degradation of SMARCA2 in mouse lung cancer xenograft models that leads to tumour growth inhibition. At the same time, ACBI2 offers a clear window of selectivity between SMARCA2 and SMARCA4 degradation in human whole blood and a consistent preference for the degradation of SMARCA2 over SMARCA4 in cell lines expressing both ATPases. Nevertheless, it is notable that despite efficient degradation of SMARCA2 *in vivo*, only tumour stasis was observed upon compound treatment in the models studied therein. This is unexpected given the strong effects observed upon SMARCA2 deletion or knockdown in functional genomic studies[5–7], suggesting a disconnect with pharmacological degradation. While it cannot entirely be excluded that more efficacious degraders may cause stronger effects, it is also possible that cells can more readily adapt to loss of SMARCA2 and SMARCA4 *in vivo* than *in vitro*, highlighting the need for *in vivo* validation of therapeutic concepts. The possibility that other indications such as prostate cancer or multiple myeloma are more dependent dual loss of SMARCA2 and SMARCA4 remains[25]. In either case, appropriate drug combinations could enhance *in vivo* efficacy and warrant dedicated investigation in the future. To promote further understanding in the community, ACBI2 will be made available upon request via the opnMe innovation platform (https://opnme.com/). We anticipate that our study will induce a significant shift in thinking around the design of orally efficacious bifunctional molecules and hope that the studies described here will encourage others to explore the chemical and biological space that may be utilised to discover orally active bifunctional small molecule therapeutics.

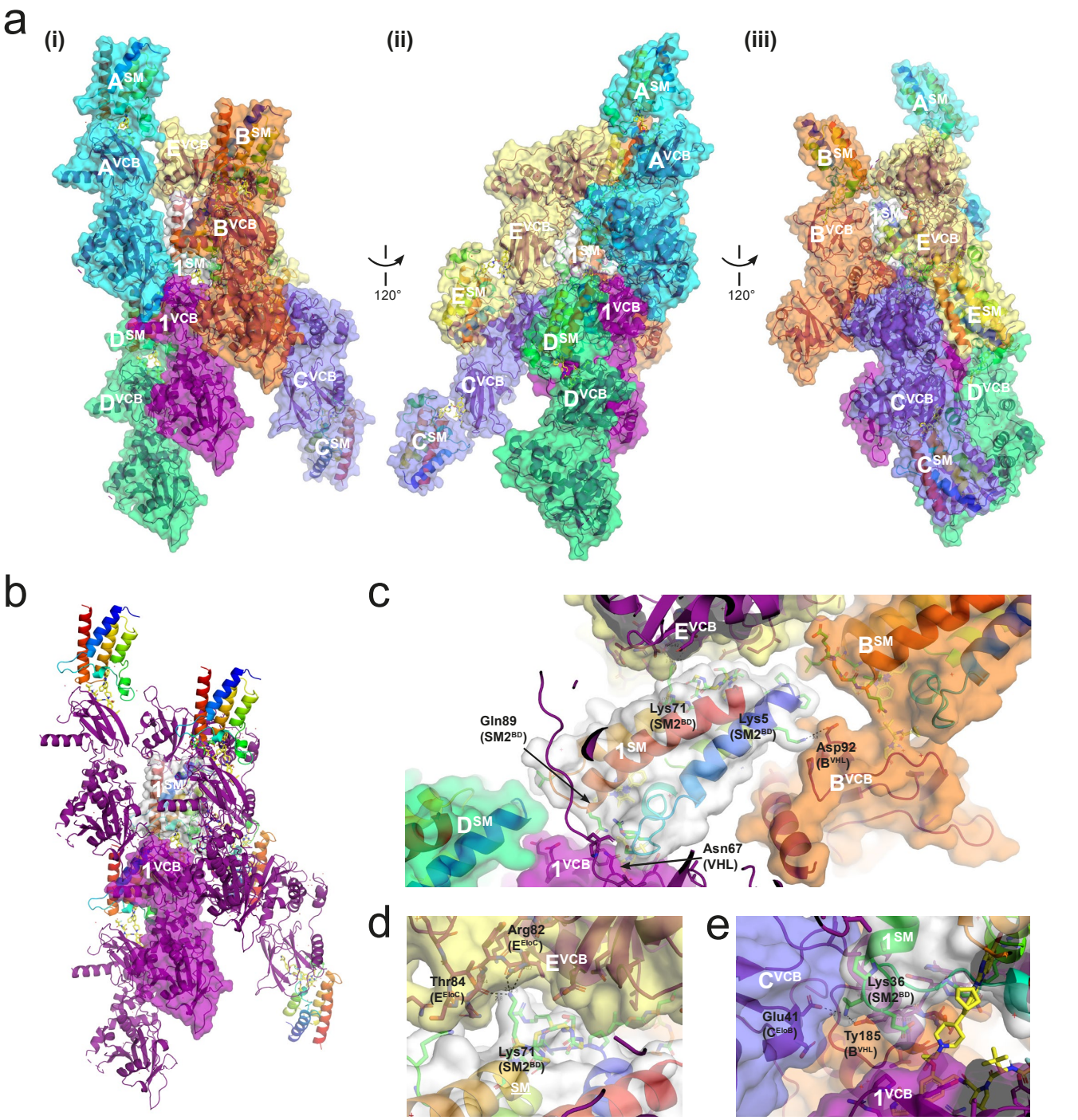

Extended Data Figure 1. Close crystal packing in the VCB : compound 5 : SMARCA2^{BD} ternary complex crystal structure. Cartoon and surface representation showing central single copy (1) of the VCB : compound **5** : SMARCA2^{BD} ternary complex comprising the asymmetric unit (asu), surrounded by closely packed symmetry-related copies (A-E, surface coloured teal, orange, blue, green, yellow respectively in panel **a**). Panels **a(i)** and **b** show the identical orientation, however in **b** for symmetry copies A-E the surface is not shown, to more clearly identify the asu (copy 1, both cartoon and surface in both panels; VCB shown as purple cartoon and surface; compound **5** shown as yellow sticks; SMARCA2^{BD}, SM, shown as rainbow cartoon from blue N-terminus to red C-terminus and light grey surface). Panels **c-e** show in closeup some of the interactions of the SMARCA2^{BD} that mediate crystal contacts, including hydrogen bond/salt bridge interactions and van der Waals interactions, in particular residues Lys5, Lys36 and Lys71 of SMARCA2^{BD}.

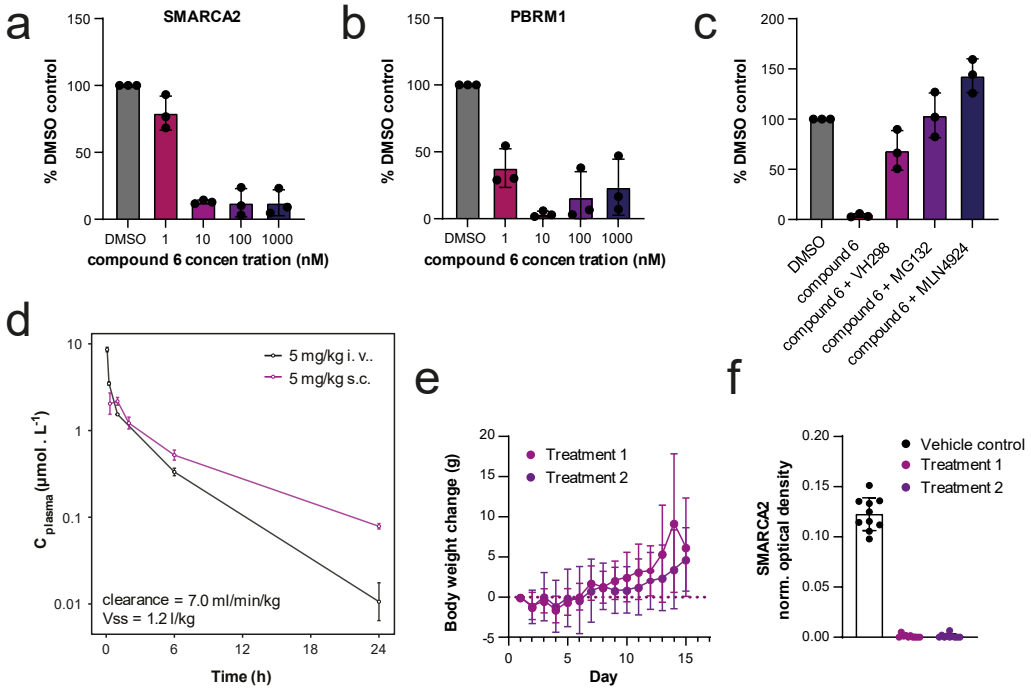

Extended Data Figure 2. Quantification of cellular and *in vivo* target protein degradation by compound 6. a. Quantified immunoblot of SMARCA2 degradation in NCI-H1568 cells treated with indicated concentrations of compound **6** for 4 h. Data was obtained from n=3 independent experiments. **b.** As **a** for PBRM1. **c.** Quantified immunoblot of SMARCA2 degradation in NCI-H1568 cells treated with 100nM compound **6** alone and in combination with 10 µM VH298, MLN4924 and MG132 for 4 h. Data was obtained from n=3 independent experiments. **d.** Plasma profiles of compound **6** in mouse after administration of 5 mg/kg i.v. or 5 mg/kg s.c. **e**. NCI-H1568 tumour bearing mice were treated subcutaneously with 5 mg/kg compound **6** with two different treatment schedules ("Treatment 1/2", see methods for details). Body weight was measured daily. Displayed are mean and standard deviation of change per day for n=10 animals. **f**. Tumours from **e** were collected at the end of the study and SMARCA2 levels in viable tumour tissue were determined using DAB-based IHC staining. Each datapoint represents the background-normalised DAB optical density (OD) within the viable tumour area of one tumour section, corresponding to an individual tumour. Mean OD levels and standard deviations are indicated in the graphs. In most cases, SMARCA2 levels in tumours from treated animals were below the limit of detection.

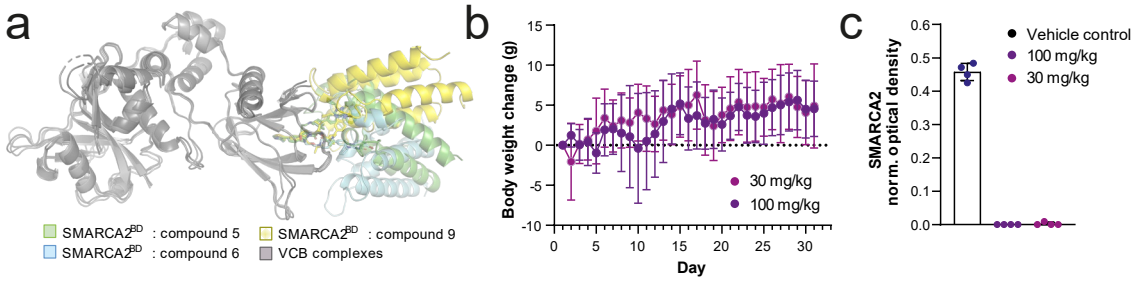

Extended Data Figure 3. Tolerability and biomarker modulation of compound 10 after oral administration. a. Superposition of ternary PROTAC complexes showing close overlap of VCB complexes (gray) and different orientations for SMARCA2^{BD} with compound **9** (yellow), compound **5** (green) and compound **6** (blue). **b.** NCI-H1568 tumour bearing mice were treated orally with compound **10** at 30 or 100 mg/kg daily. Average tumour volume at the beginning of treatment was ~220 mm^3. Body weight was measured daily. Displayed are mean and standard deviation of change per day for n=10 animals. **c**. Tumours from **b** were collected at the end of the study and SMARCA2 levels in viable tumour tissue from four animals per group were determined using DAB-based IHC staining. Each datapoint represents the background-normalised DAB optical density (OD) within the viable tumour area of one tumour section, corresponding to an individual tumour. Mean OD levels and standard deviations are indicated in the graphs. In most cases, SMARCA2 levels in tumours from treated animals were below the limit of detection.

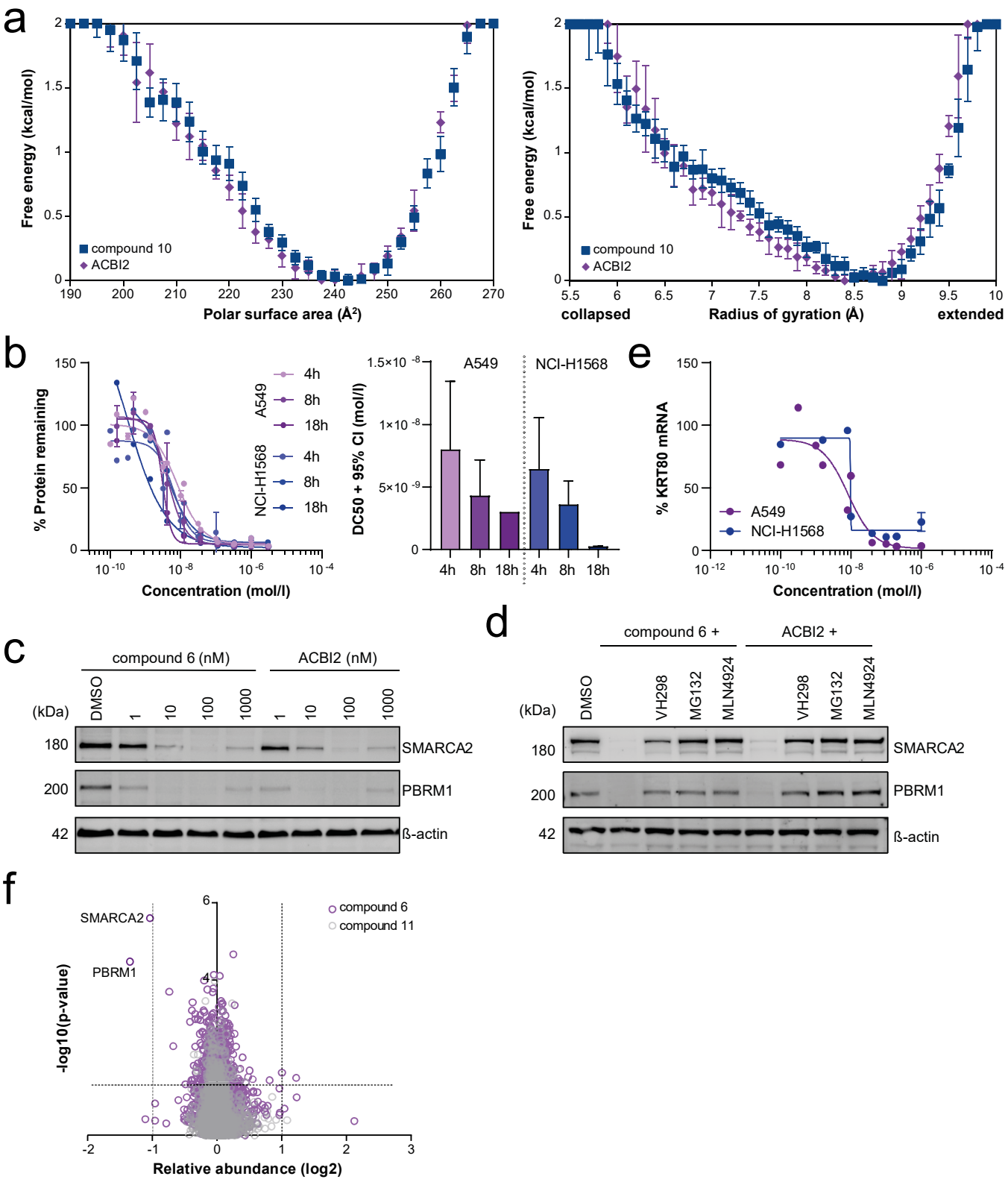

Extended Data Figure 4. Characterisation of ACBI2 by molecular dynamics, cellular degradation, qPCR assays and unbiased proteomics. a. Free energy profiles from MD simulations for ACBI2 compared to compound **10**. **b.** A549 and NCI-H1568 cells were treated with ACBI2 at the indicated concentrations for the indicated times, and remaining SMARCA2 protein levels were determined by capillary electrophoresis relative to DMSO control.

Displayed are means of 1-3 independent experiments, error bars indicate standard deviation. Right panel shows DC_{50} values with 95% confidence interval from 4-parametric logistic curve fit. **c.** Immunoblot of SMARCA2 and PBRM1 degradation in NCI-H1568 cells treated with indicated concentrations of compound **6** and ACBI2 for 4 h. **d.** Immunoblot of SMARCA2 and PBRM1 degradation in NCI-H1568 cells treated with 100 nM compound **6** and ACBI2 alone and in combination (indicated by +) with 10 µM VH298, MLN4924 and MG132 for 4 h. **e.** qPCR for *KRT80* mRNA levels (normalised to GAPDH housekeeping gene) after 18 h ACBI2 treatment at the indicated concentrations in A549 and NCI-H1568 cells. Means of 2 independent experiments are displayed relative to the DMSO control, error bars indicate standard deviation. **f**. Effects of compound **6** (purple) and negative control compound **11** (gray, *cis*-hydroxyproline analogue of compound **6** which is not capable of binding VHL) on the proteome of NCI-H1568 cells treated with the compounds at 100 nM for 4 h. Data are plotted as the log_2 of the normalised fold change in abundance against $–log_{10}$ of the p-value per protein from 3 independent experiments. All *t*-tests performed were two-tailed assuming equal variances.

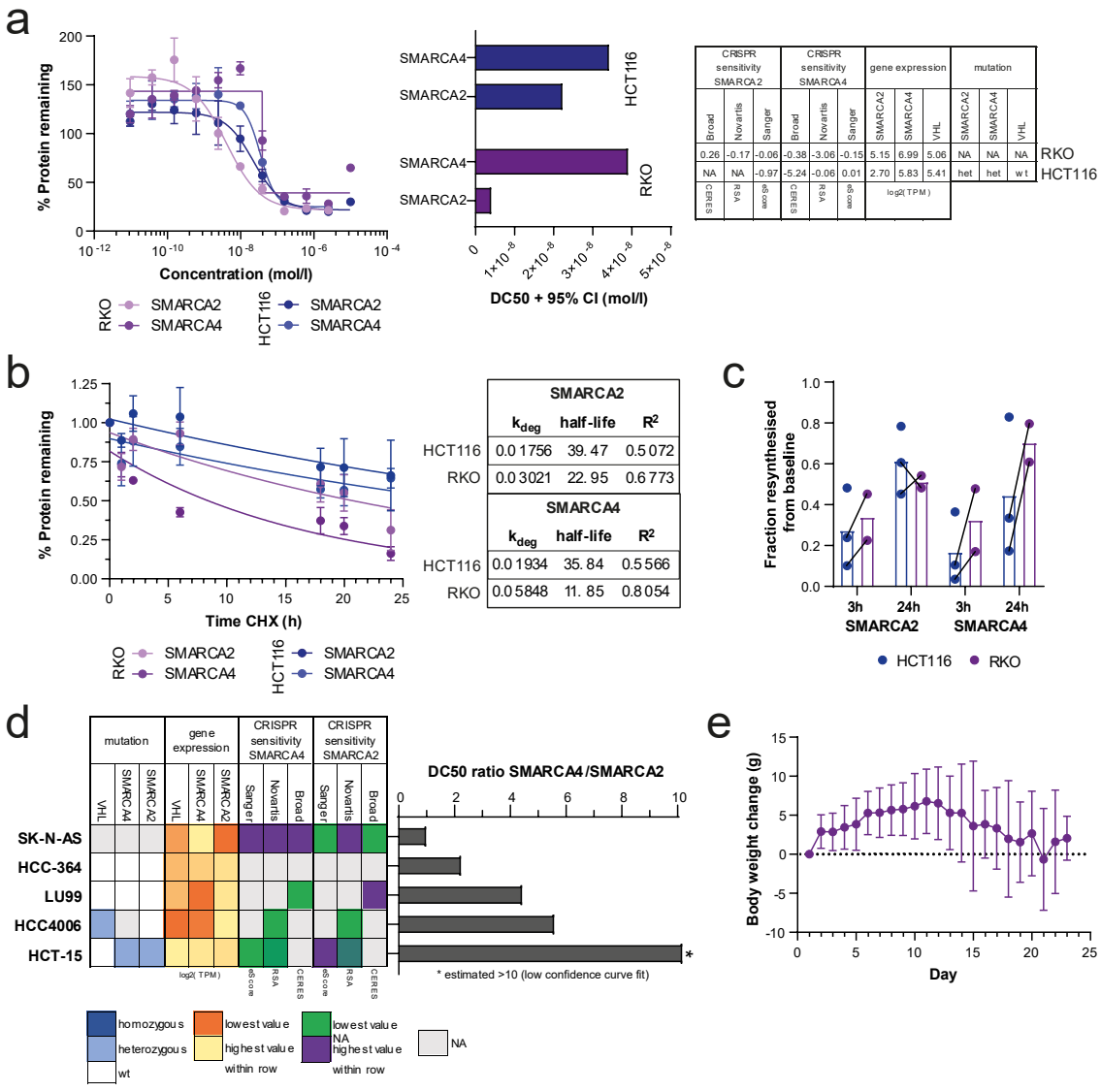

Extended Data Figure 5. Characterisation of ACBI2 in SMARCA2/4 expressing cancer cell lines and *in vivo* tolerability. a. RKO and HCT116 cells were treated with ACBI2 at the indicated concentrations for 18 h, and remaining SMARCA2/4 protein levels were determined by capillary electrophoresis relative to DMSO control. Displayed are means of 2 independent experiments, error bars indicate standard deviation. Right panel shows

DC_{50} values with 95% confidence interval from 4-parametric logistic curve fit. Table provides sensitivity to genetic depletion by CRISPR, gene expression and mutation data from DepMap/CCLE. **b.** SMARCA2/4 half-life after cycloheximide treatment for the indicated duration in HCT116 and RKO cells. Protein levels were determined by capillary electrophoresis and were displayed relative to respective DMSO controls (means of 3 independent experiments, error bars indicate standard deviation). Table shows curve fit parameters (degradation rate, half-life and goodness of fit) from one-phase exponential decay. **c.** SMARCA2/4 re-synthesis after degradation with 100 nM compound **6** for 4 h (= baseline) and blocking with a VHL inhibitor (compound **32**, 25-50 µM) for 3 or 24 h. Baseline values were subtracted from DMSO control values and set to 1. 3 and 24 h time points are displayed as fractions of this. n=2-3 independent experiments. **d.** As in **a** for SMARCA2/4 in the indicated cell lines after ACBI2 treatment. Displayed are ratios of SMARCA4 over SMARCA2 DC_{50} values obtained from 4-parametric logistic curve fits of 2-5 independent experiments. Heatmap provides sensitivity to genetic depletion by CRISPR, gene expression and mutation data from DepMap/CCLE, scaled for each row, i.e. across cell lines, but separate for each parameter. **e.** A549 tumour bearing mice were treated orally with 80 mg/kg ACBI2 once daily. Average tumour volume at the start of treatment was ~220 mm^3. Body weight was measured daily. Displayed are mean and standard deviation of change per day for n=10 animals.

1

SPR												
Sample Code	VCB KD (nM)	VCB t1/2 (s)	VCB + SMARCA2 KD (nM)	VCB_SMARCA2 t1/2 (s)	alpha	VCB + SMARCA4 KD (nM)	VCB SMARCA4 t1/2 (s)	alpha	SMARCA2 KD (nM)	SMARCA2 t1/2 (s)	SMARCA4 KD (nM)	SMARCA4 t1/2 (s)
compound 1	-	-	-	-	-	-	-	-	1058 ± 258 (n = 3)	1.4	1683 ± 317 (n = 3)	1.3
compound 2	-	-	-	-	-	-	-	-	1159 ± 421 (n = 6)	3.7	2750 ± 455 (n = 5)	-
compound 3	-	-	-	-	-	-	-	-	46 ± 5 (n = 3)	7.7	58 ± 10 (n = 3)	6.5
compound 4	-	-	-	-	-	-	-	-	-	-	-	-
compound 5	24 ± 22 (n = 4)	86.7	340 ± 71 (n = 3)	26.7	0.1	182 ± 6 (n = 3)	30.1	0.1	79 ± 17 (n = 3)	15.3	136 ± 27 (n = 3)	10.4
compound 6	11 ± 5 (n = 4)	67.1	17 ± 2 (n = 3)	113.8	0.6	9 ± 1 (n = 3)	135.2	1.2	79 ± 8 (n = 3)	16.6	124 ± 22 (n = 3)	11.7
compound 7	28 ± 13 (n = 4)	30.3	50 ± 9 (n = 3)	68.4	0.6	46 ± 2 (n = 3)	47	0.6	148 ± 17 (n = 3)	4.8	235 ± 13 (n = 3)	4.1
compound 8	34 ± 6 (n = 4)	28.2	210 ± 83 (n = 3)	42.6	0.2	180 ± 13 (n = 3)	26.3	0.2	263 ± 9 (n = 3)	3.1	505 ± 184 (n = 3)	4.9
compound 9	124 ± 97 (n = 4)	18.7	159 ± 80 (n = 3)	70.1	0.8	172 ± 115 (n = 3)	19.1	0.7	222 ± 6 (n = 3)	3.7	381 ± 28 (n = 3)	2.7
compound 10	9 ± 3 (n = 9)	133	37 ± 12 (n = 2)	103	0.3	18 ± 2 (n = 3)	105.6	0.6	144 ± 4 (n = 3)	9.4	297 ± 147 (n = 3)	6.5
ACBI2	28 ± 35 (n = 8)	117.7	44 ± 11 (n = 3)	87.3	0.8	24 ± 4 (n = 3)	95.3	1.4	208 ± 39 (n = 3)	24.9	314 ± 76 (n = 3)	11.4
compound 11	>2,000 (n = 2)	-	-	-	-	-	-	-	81 ± 3 (n = 3)	17.8	147 ± 11 (n = 3)	12.2

compound 12	629 ± 88 (n = 2)	-	-	-	-	-	-	-	214 ± 15 (n = 3)	10.7	362 ± 52 (n = 3)	7.6
compound 13	-	-	-	-	-	-	-	-	24533 ± 2173 (n = 3)	-	35600 ± 346 (n = 3)	-
compound 14	-	-	-	-	-	-	-	-	-	-	-	-
compound 15	-	-	-	-	-	-	-	-	9003 ± 526 (n = 3)	-	11967 ± 902 (n = 3)	-
compound 16	-	-	-	-	-	-	-	-	17900 ± 917 (n = 3)	-	22067 ± 1234 (n = 3)	-
compound 17	-	-	-	-	-	-	-	-	-	-	-	-
compound 18	-	-	-	-	-	-	-	-	558 ± 132 (n = 3)	8.8	672 ± 85 (n = 3)	7.3
compound 19	-	-	-	-	-	-	-	-	64 ± 4 (n = 3)	25.7	138 ± 43 (n = 3)	11.4
compound 20	9 ± 7 (n = 4)	155.4	97 ± 10 (n = 3)	31.8	0.1	67 ± 3 (n = 3)	38.4	0.1	104 ± 6 (n = 3)	11.3	182 ± 23 (n = 3)	7.5
compound 21	21 ± 5 (n = 4)	26.9	58 ± 8 (n = 3)	39.2	0.4	16 ± 11 (n = 3)	58.1	1.3	680 ± 121 (n = 3)	1.5	863 ± 179 (n = 3)	-
compound 22	39 ± 16 (n = 4)	21.5	77 ± 14 (n = 3)	52.9	0.5	26 ± 2 (n = 3)	93.2	1.5	1102 ± 433 (n = 3)	1.5	1430 ± 339 (n = 3)	1.9
compound 23	16 ± 8 (n = 4)	97.6	120 ± 8 (n = 3)	23.3	0.1	84 ± 1 (n = 3)	30.4	0.2	94 ± 11 (n = 3)	15.3	169 ± 76 (n = 3)	16.6
compound 24	-	-	-	-	-	-	-	-	-	-	-	-
compound 25	6 ± 1	82.9	36 ± 15	75.3	0.2	14 ± 2	96.8	0.4	93 ± 3	10.6	153 ± 10	3.6

	(n = 3)		(n = 3)			(n = 3)			(n = 3)		(n = 3)	
compound 26	76 ± 46 (n = 4)	16.4	95 ± 37 (n = 3)	81.4	0.8	116 ± 16 (n = 3)	32.1	0.7	118 ± 5 (n = 3)	6.7	210 ± 17 (n = 3)	4.5
compound 27	12 ± 9 (n = 4)	75	26 ± 0 (n = 3)	72.5	0.5	18 ± 1 (n = 3)	66.2	0.7	217 ± 30 (n = 3)	3.7	388 ± 96 (n = 3)	2.8
compound 28	55 ± 29 (n = 9)	25.4	120 ± 34 (n = 3)	70.2	0.5	73 ± 13 (n = 3)	76.8	0.8	196 ± 3 (n = 3)	5.4	278 ± 14 (n = 3)	4
compound 29	13 ± 7 (n = 6)	92.2	20 ± 4 (n = 3)	141.7	0.6	11 ± 1 (n = 3)	141.1	1.1	255 ± 42 (n = 3)	9.1	397 ± 49 (n = 3)	6.5
compound 30	29 ± 8 (n = 4)	55.7	86 ± 22 (n = 3)	62.1	0.3	45 ± 6 (n = 3)	65.1	0.6	325 ± 31 (n = 3)	11.5	579 ± 89 (n = 3)	7.8
compound 31	37 ± 28 (n = 4)	38	175 ± 79 (n = 3)	27.4	0.2	69 ± 8 (n = 3)	34.1	0.5	45 ± 3 (n = 3)	21.2	92 ± 17 (n = 3)	13.3

Extended Data Table 1: Measurement of binding affinities, cooperativities and ternary complex half-lives *via* SPR, errors are ± standard deviation with repeats (*n*) specified in brackets.

1

Compound	Cellular degradation / proliferation										
	RKO (18 h) SMARCA2 DC_{50} (nM)	RKO (18 h) SMARCA2 D_{max} (%)	RKO (18 h) SMARCA4 DC_{50} (nM)	RKO (18 h) SMARCA4 D_{max} (%)	RKO (4 h) SMARCA2 DC_{50} (nM)	RKO (4 h) SMARCA2 D_{max} (%)	RKO (4 h) SMARCA4 DC_{50} (nM)	RKO (4 h) SMARCA4 D_{max} (%)	NCI-H1568 (4 h) SMARCA2 DC_{50} (nM)	NCI-H1568 (18 h) SMARCA2 D_{max} (%)	NCI-H1568 (18 h) CTG (nM)
compound 1	>25,000 (n = 3)	-	>25,000 (n = 3)	-	>25,000 (n = 3)	-	>25,000 (n = 3)	-	-	-	1,097 ± 2,505 (n = 3)
compound 2	>25,000 (n = 3)	-	>25,000 (n = 3)	-	>25,000 (n = 3)	-	>25,000 (n = 3)	-	-	-	>10,000 (n = 3)
compound 3	22,348 ± 2,456 (n = 3)	-	11,377 ± 4,483 (n = 3)	82 ± 32 (n = 3)	>25,000 (n = 3)	-	>25,000 (n = 3)	-	>2,500 (n = 3)	-	1,259 ± 1,644 (n = 6)
compound 4	-	-	-	-	-	-	-	-	-	-	-
compound 5	78 ± 31 (n = 3)	46 ± 9 (n = 3)	>25,000 (n = 3)	-	>25,000 (n = 3)	-	>25,000 (n = 3)	-	-	-	175 ± 40 (n = 3)
compound 6	1 ± 1 (n = 2)	84 ± 4 (n = 2)	6 ± 2 (n = 3)	89 ± 4 (n = 3)	2 ± 1 (n = 3)	77 ± 6 (n = 3)	5 ± 2 (n = 4)	86 ± 5 (n = 4)	5 ± 3 (n = 3)	94 ± 5 (n = 3)	2 ± 750 (n = 37)
compound 7	10 ± 2 (n = 3)	80 ± 8 (n = 3)	>25,000 (n = 3)	-	23 ± 8 (n = 4)	75 ± 8 (n = 3)	>25,000 (n = 3)	-	50 ± 7 (n = 3)	85 ± 4 (n = 3)	25 ± 19 (n = 6)
compound 8	5 ± 1 (n = 1)	76 ± 10 (n = 3)	1,779 ± 1,802 (n = 2)	88 ± 16 (n = 2)	12 ± 4 (n = 4)	72 ± 7 (n = 4)	>25,000 (n = 4)	-	32 ± 17 (n = 3)	92 ± 8 (n = 3)	45 ± 51 (n = 3)
compound 9	3 ± 3 (n = 3)	82 ± 5 (n = 3)	174 ± 72 (n = 3)	68 ± 15 (n = 3)	6 ± 3 (n = 4)	70 ± 2 (n = 4)	83 ± 22 (n = 2)	34 ± 6 (n = 2)	-	-	16 ± 7 (n = 3)
compound 10	1 ± 0.1 (n = 4)	87 ± 2 (n = 4)	12 ± 3 (n = 5)	78 ± 11 (n = 5)	2 ± 1 (n = 4)	73 ± 6 (n = 4)	15 ± 9 (n = 4)	53 ± 16 (n = 4)	8 ± 4 (n = 3)	90 ± 0.3 (n = 3)	7 ± 3 (n = 6)
ACBI2	1 ± 1	81 ± 7	32 ± 12	67 ± 8	4 ± 1	71 ± 2	>25,000	-	13 ± 14	86 ± 6	7 ± 4

	(n = 7)	(n = 7)	(n = 9)	(n = 9)	(n = 4)	(n = 4)	(n = 4)		(n = 3)	(n = 3)	(n = 6)
compound 11	10,423 ± 7,064 (n = 3)	93 ± 12 (n = 3)	8,162 ± 1,347 (n = 3)	91 ± 8 (n = 3)	>25,000 (n = 3)	-	>25,000 (n = 3)	-	-	-	416 ± 319 (n = 6)
compound 12	7,516 423 ± 2,993 (n = 3)	82 ± 16 (n = 3)	5,828 ± 1,535 (n = 3)	94 ± 7 (n = 3)	>25,000 (n = 3)	-	>25,000 (n = 3)	-	-	-	236 ± 175 (n = 6)
compound 13	>25,000 (n = 3)	-	>25,000 (n = 3)	-	>25,000 (n = 3)	-	>25,000 (n = 3)	-	-	-	>10,000 (n = 6)
compound 14	>25,000 (n = 3)	-	>25,000 (n = 3)	-	>25,000 (n = 3)	-	>25,000 (n = 3)	-	-	-	>10,000 (n = 6)
compound 15	>25,000 (n = 3)	-	>25,000 (n = 3)	-	>25,000 (n = 3)	-	>25,000 (n = 3)	-	-	-	>10,000 (n = 6)
compound 16	>25,000 (n = 3)	-	>25,000 (n = 3)	-	>25,000 (n = 3)	-	>25,000 (n = 3)	-	-	-	>10,000 (n = 6)
compound 17	>25,000 (n = 3)	-	>25,000 (n = 3)	-	>25,000 (n = 3)	-	>25,000 (n = 3)	-	-	-	>10,000 (n = 6)
compound 18	>25,000 (n = 3)	-	>25,000 (n = 3)	-	>25,000 (n = 3)	-	>25,000 (n = 3)	-	-	-	>10,000 (n = 3)
compound 19	>25,000 (n = 3)	-	>25,000 (n = 3)	-	>25,000 (n = 3)	-	>25,000 (n = 3)	-			564 ± 384 (n = 3)
compound 20	>25,000 (n = 3)	-	>25,000 (n = 3)	-	>25,000 (n = 3)	-	>25,000 (n = 3)	-	>2,500 (n = 3)	-	74 ± 52 (n = 3)
compound 21	106 ± 38 (n = 3)	67± 8 (n = 3)	83 ± 78 (n = 3)	75 ± 3 (n = 3)	>25,000 (n = 3)	-	21 ± 19 (n = 3)	61 ± 16 (n = 3)	-	-	223 ± 30 (n = 3)
compound 22	148 ± 97 (n = 3)	75 ± 8 (n = 3)	77 ± 67 (n = 3)	89 ± 5 (n = 3)	175 ± 165 (n = 3)	71 ± 25 (n = 3)	54 ± 47 (n = 3)	84 ± 1 (n = 3)	-	-	187 ± 76 (n = 3)

compound 23	39 ± 10 (n = 3)	37 ± 5 (n = 3)	1,260 ± 2,657 (n = 3)	76 ± 30 (n = 3)	>25,000 (n = 3)	-	>25,000 (n = 3)	-	-	-	104 ± 27 (n = 3)
compound 24	-	-	-	-	-	-	-	-	-	-	-
compound 25	3 ± 1 (n = 3)	80 ± 6 (n = 2)	40 ± 16 (n = 3)	52 ± 21 (n = 3)	3 ± 1 (n = 3)	66 ± 5 (n = 3)	83 ± 22 (n = 2)	34 ± 6 (n = 2)	-	-	7 ± 4 (n = 3)
compound 26	6 ± 2 (n = 3)	82 ± 4 (n = 3)	83 ± 21 (n = 3)	82 ± 5 (n = 3)	12 ± 7 (n = 4)	77 ± 3 (n = 4)	81 ± 14 (n = 3)	61 ± 15 (n = 3)	-	-	33 ± 25 (n = 3)
compound 27	2 ± 1 (n = 3)	85 ± 3 (n = 3)	29 ± 6 (n = 3)	83 ± 7 (n = 3)	5 ± 2 (n = 4)	70 ± 7 (n = 4)	42 ± 3 (n = 3)	55 ± 2 (n = 3)	-	-	13 ± 1 (n = 3)
compound 28	5 ± 2 (n = 4)	76 ± 11 (n = 4)	159 ± 57 (n = 3)	14 ± 42 (n = 3)	17 ± 8 (n = 4)	69 ± 4 (n = 4)	>25,000 (n = 4)	-	18 ± 13 (n = 3)	94 ± 6 (n = 3)	16 ± 5 (n = 6)
compound 29	1 ± 0.1 (n = 4)	84 ± 4 (n = 4)	11 ± 3 (n = 6)	87 ± 6 (n = 9)	2 ± 1 (n = 4)	74 ± 2 (n = 4)	15 ± 6 (n = 4)	68 ± 6 (n = 4)	-	-	5 ± 2 (n = 5)
compound 30	3 ± 1 (n = 4)	82 ± 5 (n = 4)	73 ± 35 (n = 3)	72 ± 7 (n = 3)	8 ± 2 (n = 2)	74 ± 5 (n = 2)	>25,000 (n = 3)	-	-	-	12 ± 6 (n = 4)
compound 31	3 ± 1 (n = 3)	83 ± 4 (n = 3)	29 ± 15 (n = 3)	76 ± 4 (n = 3)	4 ± 0.2 (n = 4)	72 ± 7 (n = 4)	18 ± 14 (n = 4)	53 ± 15 (n = 4)	-	-	18 ± 7 (n = 3)

Extended Data Table 2: Measurement of target protein degradation (all columns except rightmost) or cell proliferation (rightmost column; CTG, CellTiter Glo) in cancer cell lines. Data represent means with errors stated as ± standard deviation with repeats (*n*) specified in brackets.

1

2

Compound	TR-FRET								
	SMARCA2^{BD} IC_{50} (nM)	Ternary SMARCA2^{BD} IC_{50} (nM) (PROTAC + VCB)	α	SMARCA4^{BD} IC_{50} (nM)	Ternary SMARCA4^{BD} IC_{50} (nM) (PROTAC + VCB)	α	PBRM1^{BD} IC_{50} (nM)	Ternary PBRM1^{BD} IC_{50} (nM) (PROTAC + VCB)	α
compound 1	425 ± 11 (n = 3)	389 ± 31 (n = 3)	-	857 ± 64 (n = 3)	844 ± 42 (n = 3) -	-	134 ± 28 (n = 3)	131 ± 8 (n = 3)	-
compound 2	1,774 ± 254 (n = 4)	1,954 ± 393 (n = 4)	-	2,400 ± 417 (n = 3)	2,321 ± 257 (n = 3)	-	1,000 ± 75 (n = 3)	959 ± 53 (n = 3)	-
compound 3	48 ± 17 (n = 189)	48 ± 17 (n = 189)	-	107 ± 29 (n = 40)	108 ± 30 (n = 43)	-	31 ± 12 (n = 42)	31 ± 11 (n = 43)	-
compound 4	88 (n = 1)	74 (n = 1)	1.2 (n = 1)	-	-	-	-	-	-
compound 5	98 ± 17 (n = 4)	127 ± 43 (n = 4)	0.8 ± 0.2 (n = 4)	203 ± 29 (n = 4)	226 ± 67 (n = 4)	0.9 ± 0.2 (n = 4)	42 ± 3 (n = 4)	20 ± 3 (n = 4)	2.0 ± 0.2 (n = 4)
compound 6	57 ± 11 (n = 9)	14 ± 5 (n = 7)	4.1 ± 1.2 (n = 7)	127 ± 39 (n = 5)	44 ± 14 (n = 5)	2.9 ± 0.1 (n = 5)	20 ± 5 (n = 6)	2 ± 0.4 (n = 6)	9.6 ± 2.6 (n = 6)
compound 7	82 ± 17 (n = 10)	25 ± 19 (n = 10)	3.9 ± 1.0 (n = 9)	189 ± 25 (n = 5)	100 ± 45 (n = 6)	1.8 ± 0.4 (n = 5)	30 ± 3 (n = 5)	6 ± 1 (n = 5)	5.3 ± 0.5 (n = 5)
compound 8	143 ± 27 (n = 9)	21 ± 5 (n = 10)	7.0 ± 2.6 (n = 9)	265 ± 34 (n = 3)	105 ± 20 (n = 5)	2.2 ± 0.2 (n = 3)	34 ± 4 (n = 5)	7 ± 3 (n = 6)	5.5 ± 1.7 (n = 5)
compound 9	150 ± 52 (n = 6)	15 ± 9 (n = 7)	10.1 ± 3.8 (n = 6)	191 ± 85 (n = 3)	70 ± 16 (n = 4)	2.6 ± 0.8 (n = 3)	31 ± 1 (n = 3)	8 ± 1 (n = 4)	4.2 ± 0.4 (n = 3)
compound 10	123 ± 45 (n = 13)	25 ± 6 (n = 11)	5.3 ± 2.1 (n = 10)	279 ± 40 (n = 3)	67 ± 9 (n = 3)	4.2 ± 0.4 (n = 3)	41 ± 8 (n = 4)	4 ± 1 (n = 3)	11.9 ± 1.3 (n = 3)

ACBI2	172 ± 109 (n = 5)	42 ± 2 (n = 5)	4.6 ± 2.2 (n = 10)	314 ± 121 (n = 3)	86 ± 11 (n = 3)	3.7 ± 0.8 (n = 3)	67 ± 9 (n = 3)	5 ± 1 (n = 3)	13.8 ± 1.5 (n = 3)
compound 11	76 ± 4 (n = 3)	80 ± 5 (n = 3)	1.0 ± 0.0 (n = 3)	147 ± 15 (n = 3)	165 ± 13 (n = 3)	0.9 ± 0.0 (n = 3)	24 ± 2 (n = 3)	29 ± 3 (n = 3)	0.8 ± 0.1 (n = 3)
compound 12	203 ± 65 (n = 4)	181 ± 44 (n = 4)	1.1 ± 0.3 (n = 4)	347 ± 41 (n = 3)	367 ± 38 (n = 3)	0.9 ± 0.1 (n = 3)	75 ± 6 (n = 3)	78 ± 7 (n = 3)	1.0 ± 0.0 (n = 3)
compound 13	>10,000 (n = 3)	-	-	>10,000 (n = 3)	-	-	>10,000 (n = 3)	-	-
compound 14	>10,000 (n = 3)	-	-	>10,000 (n = 3)	-	-	>10,000 (n = 3)	-	-
compound 15	>10,000 (n = 3)	-	-	>10,000 (n = 3)	-	-	>10,000 (n = 3)	-	-
compound 16	>10,000 (n = 3)	-	-	>10,000 (n = 3)	-	-	>10,000 (n = 3)	-	-
compound 17	>10,000 (n = 3)	-	-	>10,000 (n = 3)	-	-	>10,000 (n = 3)	-	-
compound 18	47 (n = 1)	43 (n = 1)	-	-	-	-	-	-	-
compound 19	85 ± 7 (n = 3)	72 ± 3 (n = 3)	1.2 ± 0.1 (n = 3)	158 ± 27 (n = 3)	173 ± 19 (n = 3)	0.9 ± 0.1 (n = 3)	38 ± 2 (n = 3)	40 ± 1 (n = 3)	1.0 ± 0.1 (n = 3)
compound 20	78 ± 20 (n = 5)	141 ± 42 (n = 5)	0.6 ± 0.2 (n = 5)	120 ± 17 (n = 4)	309 ± 11 (n = 4)	0.4 ± 0.0 (n = 4)	38 ± 4 (n = 4)	35 ± 4 (n = 4)	1.1 ± 0.1 (n = 4)
compound 21	255 ± 9 (n = 3)	134 ± 11 (n = 3)	1.9 ± 0.1 (n = 3)	520 ± 73 (n = 3)	130 ± 13 (n = 3)	4.0 ± 0.2 (n = 3)	76 ± 4 (n = 3)	38 ± 4 (n = 3)	2.0 ± 0.1 (n = 3)
compound 22	274 ± 41 (n = 4)	102 ± 27 (n = 4)	2.8 ±0.8 (n = 4)	813 ± 126 (n = 4)	89 ± 13 (n = 4)	9.1 ± 0.7 (n = 4)	103 ± 13 (n = 4)	38 ± 5 (n = 3)	2.6 ± 0.1 (n = 4)

compound 23	98 ± 12 (n = 4)	164 ± 124 (n = 4)	0.7 ± 0.3 (n = 4)	174 ± 21 (n = 4)	206 ± 51 (n = 4)	0.9 ± 0.1 (n = 4)	39 ± 5 (n = 4)	21 ± 3 (n = 4)	2.0 ± 0.4 (n = 4)
compound 24	-	-	-	-	-	-	-	-	-
compound 25	87 ± 35 (n = 14)	43 ± 48 (n = 13)	2.2 ± 0.6 (n = 12)	182 ± 57 (n = 4)	79 ± 9 (n = 4)	2.3 ± 0.4 (n = 4)	36 ± 12 (n = 5)	3 ± 1 (n = 5)	11.2 ± 2.1 (n = 5)
compound 26	71 ± 15 (n = 11)	13 ± 5 (n = 11)	5.8 ± 1.9 (n = 11)	149 ± 41 (n = 9)	56 ± 23 (n = 10)	2.6 ± 0.7 (n = 3)	22 ± 5 (n = 10)	6 ± 2 (n = 8)	4.0 ± 1.2 (n = 8)
compound 27	91 ± 11 (n = 9)	29 ± 8 (n = 8)	3.3 ± 0.8 (n = 8)	193 ± 15 (n = 6)	69 ± 12 (n = 6)	2.8 ± 0.5 (n = 6)	33 ± 7 (n = 7)	3 ± 0.5 (n = 7)	12.2 ± 2.8 (n = 7)
compound 28	130 ± 18 (n = 10)	35 ± 4 (n = 10)	3.8 ± 0.4 (n = 10)	240 ± 55 (n = 4)	76 ± 21 (n = 4)	3.2 ± 0.7 (n = 4)	24 ± 11 (n = 4)	4 ± 2 (n = 4)	6.9 ± 1.9 (n = 4)
compound 29	201 ± 45 (n = 4)	32 ± 2 (n = 4)	6.4 ± 1.1 n = 4)	416 ± 177 (n = 3)	60 ± 12 (n = 3)	7.0 ± 1.3 (n = 3)	85 ± 25 (n = 3)	3 ± 1 (n = 3)	24.9 ± 2.4 (n = 3)
compound 30	260 ± 100 (n = 5)	51 ± 10 (n = 5)	5.9 ± 1.9 (n = 4)	>2,000 (n = 3)	106 ± 16 (n = 3)	4.3 ± 0.5 (n = 3)	131 ± 49 (n = 3)	6 ± 2 (n = 3)	22.4 ± 3.9 (n = 3)
compound 31	52 ± 11 (n = 7)	17 ± 4 (n = 7)	3.3 ± 1.5 (n = 7)	97 ± 17 (n = 5)	54 ± 20 (n = 5)	1.8 ± 0.4 (n = 5)	22 ± 5 (n = 5)	3 ± 1 (n = 5)	6.6 ± 0.5 (n = 5)

Extended Data Table 3: Measurement of PROTAC cooperativity (α) and ternary complex affinity (ternary IC_{50}) via TR-FRET – competition for $SMARCA2^{BD}$, $SMARCA4^{BD}$ and $PBRM1^{BD5}$ ± VCB respectively. PROTAC cooperativity (α) is calculated for $SMARCA2^{BD}$, $SMARCA4^{BD}$ and $PBRM1^{BD5}$ respectively ratio between their TR-FRET IC_{50} / TR-FRET IC_{50} +VCB values measured in the same run. Data represent means with errors stated as ± standard deviation with repeats (n) specified in brackets.

1

Compound	Physchem and DMPK															
	Solubility pH 4.5 (µg/mL)	Solubility pH 6.8 (µg/mL)	clogP	Caco-2 P_{ab} (10^{-6} cm/s)	Caco-2 Efflux ratio	Modified Caco-2 P_{ab} (10^{-6} cm/s)	Modified Caco-2 Efflux ratio	Modified Caco-2 + PGPi (Zosuquidar) P_{ab} (10^{-6} cm/s)	Modified Caco-2 + PGPi (Zosuquidar) Efflux ratio	Mic. Stab. Mouse (% Q_H)	Mic. Stab. Rat (% Q_H)	Mic. Stab. Human (% Q_H)	PPB fu 10% Calf (%)	PPB fu Mouse (%)	PPB fu Rat (%)	PPB fu Human (%)
compound 1	<1 (n = 1)	<1 (n = 1)	5.4	31 (n = 1)	0.8 (n = 1)	-	-	-	-	-	-	-	-	-	-	-
compound 2	<1 (n = 1)	<1 (n = 1)	3.7	37 (n = 1)	0.5 (n = 1)	-	-	-	-	-	-	-	-	-	-	-
compound 3	>110 (n = 3)	>110 (n = 3)	6.1	28 (n = 1)	0.8 (n = 1)	-	-	-	-	43 ± 10 (n = 4)	28 ± 1 (n = 4)	<24 (n = 1)	-	-	-	-
compound 4	85 (n = 1=	79 (n = 1)	5.6	-	-	-	-	-	-	<24 (n = 1)	<23 (n = 1)	<24 (n = 1)	-	-	-	-
compound 5	<1 (n = 1)	<1 (n = 1)	9.0	6 (n = 1)	1.4 (n = 1)	-	-	-	-	44 (n = 1)	31 (n = 1)	83 (n = 1)	-	-	-	-
compound 6	<1 (n = 4)	<1 (n = 4)	8.9	<0.5 (n = 2)	-	<3 (n = 3)	>63 (n = 3)	15 ± 2 (n = 3)	2 ± 0.1 (n = 3)	<24 (n = 2)	<23 (n = 2)	30 ± 2 (n = 4)	-	-	-	-
compound 7	<1 (n = 1)	<1 (n = 1)	8.9	<0.5 (n = 3)	-	2 ± 1 (n = 3)	79 ± 10 (n = 3)	10 ± 1 (n = 3)	3 ± 1 (n = 3)	38 ± 6 (n = 4)	<23 (n = 4)	66 ± 1 (n = 3)	-	-	-	-
compound 8	18 (n = 3)	<1 (n = 3)	9.2	6 ± 2 (n = 3)	5 ± 2 (n =3)	3 ± 1 (n = 3)	52 ± 11 (n = 3)	12 ± 2 (n = 3)	2 ± 0.2 (n = 3)	27 ± 3 (n = 3)	<23 (n = 3)	55 ± 1 (n = 2)	7 ± 2 (n = 2)	-	-	-
compound 9	190 (n = 2)	2 (n = 2)	9.3	6 (n = 1)	5 (n = 1)	-	-	-	-	68 ± 2 (n = 2)	51 ± 2 (n = 2)	86 (n = 1)	5 (n = 1)	-	-	-
compound 10	<1	<1	9.9	1.4 ± 0.5	7± 1	7 ± 5	30 ± 20	11 ± 3	2 ± 0.2	<24	<23	<24	0.14	<0.04	<0.04	<0.04

	(n = 8)	(n = 8)		(n =4)	(n = 4)	(n = 4)	(n = 4)	(n = 4)	(n = 4)	(n = 8)	(n = 8)	(n = 8)	(n = 1)	(n = 3)	(n = 3)	(n = 3)
ACBI2	<1 (n = 4)	<1 (n = 4)	10.3	2 ± 0.2 (n =4)	5 ± 1 (n =4)	5 ± 1 (n = 3)	9 ± 2 (n = 3)	8 ± 4 (n = 3)	2 ± 1 (n = 3)	<24 (n = 4)	<23 (n = 4)	<24 (n = 4)	0.35 (n = 1)	<0.05 (n = 1)	<0.05 (n = 3)	<0.05 (n = 3)
compound 11	<1 (n = 1)	<1 (n = 1)	8.9	-	-	-	-	-	-	<24 (n = 1)	<23 (n = 1)	<24 (n = 1)	-	-	-	-
compound 12	<1 (n = 1)	<1 (n = 1)	10.3	-	-	-	-	-	-	<24 (n = 1)	<23 (n = 1)	<24 (n = 1)	-	-	-	-
compound 13	>70 (n = 1)	>71 (n = 1)	2.1	93 (n = 1)	0.6 (n = 1)	-	-	-	-	-	-	-	-	-	-	-
compound 14	-	-	1.3	-	-	-	-	-	-	-	-	-	-	-	-	-
compound 15	>83 (n = 1)	>82 (n = 1)	2.2	-	-	-	-	-	-	-	-	-	-	-	-	-
compound 16	>97 (n = 1)	>97 (n = 1)	2.5	-	-	-	-	-	-	-	-	-	-	-	-	-
compound 17	-	-	1.5	-	-	-	-	-	-	-	-	-	-	-	-	-
compound 18	>100 (n = 2)	78 (n = 2)	5.6	-	-	-	-	-	-	69 ± 0.3 (n = 2)	51 ± 10 (n = 4)	45 (n = 1)	-	-	-	-
compound 19	<1 (n = 1)	<1 (n = 1)	8.7							68 (n = 1)	28 (n = 1)	82 (n = 1)				
compound 20	<1 (n = 5)	<1 (n = 5)	8.7	<0.4 (n = 1)	-	-	-	-	-	76 ± 2 (n = 4)	33 ± 3 (n = 5)	89 ± 7 (n = 5)	-	-	-	-
compound 21	190 (n = 3)	80 (n = 3)	8.6	<0.3 (n = 1)	-	-	-	-	-	56 ± 10 (n = 3)	45 ± 13 (n = 3)	87 ± 10 (n = 3)	-	-	-	-
compound 22	225 (n = 2)	160 (n = 2)	8.5	<0.3 (n = 1)	-	-	-	-	-	58 (n = 1)	40 (n = 1)	83 ± 13 (n = 2)	-	-	-	-

compound 23	<1 (n = 1)	<1 (n = 1)	9.1	0.4 (n = 1)	26 (n = 1)	-	-	-	-	42 (n = 1)	<23 (n = 1)	78 (n = 1)	-	-	-	-
compound 24	<1 (n = 2)	<1 (n = 2)	8.9	-	-	-	-	-	-	40 ± 2 (n = 2)	31 (n = 1)	59 ± 0.4 (n = 2)	-	-	-	-
compound 25	<1 (n = 1)	<1 (n = 1)	9.4	<4 (n = 1)	-	--	-	-	-	<24 (n = 1)	<23 (n = 1)	25 (n = 1)	0.7 (n = 1)	-	-	-
compound 26	177 (n = 3)	<1 (n = 3)	9.0	<3 (n =1)	-	-	-	-	-	>88 (n = 3)	58 ± 3 (n = 3)	86 ± 0.3 (n = 3)	-	-	-	-
compound 27	<1 (n = 4)	<1 (n = 4)	9.1	5 (n =1)	4 (n = 1)	-	-	-	-	<25 (n = 2)	<23 (n = 2)	43 ± 5 (n = 2)	-	-	-	-
compound 28	2 (n = 5)	<1 (n = 5)	9.6	5 ± 2 (n = 2)	5 ± 3 (n = 2)	<7 (n = 3)	>37 (n = 3)	12 ± 1 (n = 3)	1 ± 0.1 (n = 3)	<24 (n = 6)	<23 (n = 6)	57 ± 4 (n = 4)	2 ± 0.3 (n = 2)	<0.2 (n = 3)	<0.2 (n = 3)	<0.2 (n = 3)
compound 29	<1 (n = 2)	<1 (n = 2)	10.3	2 ± 0.2 (n =2)	3 ± 1 (n =2)	-	-	-	-	<24 (n = 2)	<23 (n = 2)	<24 (n = 2)	<0.14 (n = 1)	<0.34 (n = 1)	<0.27 (n = 1)	<0.05 (n = 1)
compound 30	<1 (n = 1)	<1 (n = 1)	10.7	<0.3 (n=1)	-	4 ± 1 (n = 3)	10 ± 3 (n = 3)	8 ± 1 (n = 3)	1 ± 0.4 (n = 3)	<24 (n = 1)	<23 (n = 2)	<24 (n = 2)	<0.07	-	-	-
compound 31	<1 (n = 2)	<1 (n = 2)	8.9	2 ± 1 (n = 2)	14 ± 7 (n = 2)	-	-	-	-	71 ± 12 (n = 1)	<23 (n = 2)	68 ± 3 (n = 2)	-	-	-	-

Extended Data Table 4:. Measurement of physicochemical properties and in vitro DMPK parameters. Mic. Stab. = microsomal stability ; PPB = plasma protein binding ; fu = fraction unbound. Data represent means with errors stated as ± standard deviation with repeats (*n*) specified in brackets.

	Compound **6**			Compound **10**				ACBI2		
Administration route	i.v.	s.c.		i.v.	p.o.			i.v.	p.o.	
Study type	PK		Biomarker	PK	Xenograft			PK	Xenograft	
Dose (mg/kg)	5	5	5	5	30	30	100	5	30	80
$AUC_{0\text{-}24h}$ (nM h)	12000	13000	12000	36000	9300	21000	38000	38000	50000	84000
$AUC_{0\text{-}inf}$ (nM h)	12000	13000	13000	36000	9400	21000	39000	38000	51000	–
Clearance (mL/min/kg)	7.1	–	–	2.2	–	–	–	2	–	–
V_{ss} (L/kg)	1.2	–	–	0.38	–	–	–	0.47	–	–
MRT (h)	2.8	6.3	7.9	2.9	5	5.6	5.1	3.8	6.1	–
Bioavailability (%)	–	110	–	–	4.3	–	–	–	22	–

Extended Data Table 5: Compound pharmacokinetics in pharmacokinetic and pharmacology studies in NMRI mice. All data represent mean of 3 animals.

Methods

Protein crystallography and protein production

Protein production for SMARCA2 and the VCB complex was done as previously described[10]. Protein crystallisation was performed using a vapor diffusion method with 96-well sitting drop plates. For the binary SMARCA2^{BD} : compound **4** complex, SMARCA2^{BD} apo crystals were soaked overnight with a 2 mM compound **4** DMSO stock solution. Apo crystals were generated by mixing 200 nL of SMARCA2 protein with an equal volume of reservoir solution consisting of 8% ethylene glycol, 25% PEG 6000, 0.1 M HEPES pH 8.0 and 10 mM zinc chloride. The compound **4** : SMARCA2^{BD} complex was refined to *R*work and *R*free values of 18.7 and 21.0%, respectively, with 99.4% of the residues in Ramachandran favoured regions as validated with MOLPROBITY.

For the VCB : compound **5** : SMARCA2^{BD} ternary complex, VCB, PROTAC and SMARCA2^{BD} were mixed in a 1:1:1 stoichiometric ratio in 20 mM HEPES, pH 7.5, 150 mM sodium chloride, 1 mM TCEP, 2% DMSO, incubated for 5 min at room temperature and concentrated to a final concentration of approximately 10 mg/ml. Drops were prepared by mixing 1 µl of the ternary complex with 1 µl of well solution and crystallised at 4°C using the hanging-drop vapor diffusion method. Crystals were obtained in 33% (v/v) glycerol ethoxylate, 0.2 M ammonium chloride, 0.1 M HEPES, pH 7.5. Harvested crystals were flash cooled in liquid nitrogen following gradual equilibration into cryo-protectant solution consisting of 25% (v/v) ethylene glycol in 35% (v/v) glycerol ethoxylate, 0.2 M ammonium chloride, 0.1 M HEPES, pH 7.5. Diffraction data were collected at Diamond Light Source beamline I24 (λ = 0.9686 Å) using a Pilatus3 6M detector and processed using XDS[26]. The crystals belonged to space group *P* 21 with unit cell parameters a = 47.3, b = 86.8, c = 59.3 Å and α = 90°, β = 98.9°, γ = 90° and contained one copy of the ternary complex per asymmetric unit. The structure was solved by molecular replacement using PHASER[27] with VCB coordinates derived from the VCB : MZ1 : Brd4BD2 complex (PDB: 5T35) and SMARCA2^{BD} (PDB: 4QY4) as search models. Subsequent iterative model building and refinement was done according to standard protocols using CCP4[28], COOT [29], and autoBUSTER (Global Phasing Ltd). The structure was refined to *R*work and *R*free values of 19.6 and 23.5%, respectively, with 98.0% of the residues in Ramachandran favoured regions as validated with MOLPROBITY[30] .Buried surface areas were calculated with PISA[31].

For the remaining ternary complexes, SMARCA2, VCB complex and the PROTAC molecule were mixed in a 1:1:1 molar ratio, concentrated to ~8 mg/mL in a buffer containing 20 mM HEPES pH 7.5, 100 mM NaCl, 1 mM TCEP and incubated with equal amounts of reservoir solution. For compound **6**, the reservoir solution was 20 % PEG 3350, 0.1 M BIS_TRIS propane pH 7.5 and 200 mM sodium formate. For compound **9**, the solution consisted of 14.5 % PEG 3350, 0.1 M BIS-TRIS propane pH 5.8 and 100 mM sodium iodide. For data collection, crystals were frozen in liquid nitrogen with the respective reservoir solution with 20-25 % ethylene glycol added. Synchrotron data was collected at the Swiss Light Source (Villigen) and processed with autoPROC[32] using STARANISO[33] for the determination of resolution limits. Model building was done in iterative cycles using COOT[29] and autoBUSTER[34]. The structure of the VCB : compound **6** : SMARCA2^{BD} complex was refined to *R*work and *R*free values of 19.3 and 25.1%, respectively, with 97.1% of the residues in Ramachandran favoured regions as validated with MOLPROBITY. The VCB : compound **9** : SMARCA2^{BD} complex was refined to *R*work and *R*free values of 17.8 and 20.2%, respectively, with 98.4% of the residues in Ramachandran favoured regions as validated with MOLPROBITY.

SPR experiments

SPR data were acquired on Biacore 8K or T200 instruments (Cytiva). Target proteins were immobilised at 25°C on CM5 chips by amine coupling (EDC/NHS, Cytiva) in HBS-P+ running buffer (pH 7.4), containing 2 mM TCEP. After surface activation with EDC/NHS (contact time 420 s, flow rate 10 µl/min) SMARCA2^{BD} and SMARCA4^{BD} at 0.01 -

0.05 mg/ml in coupling buffer (10 mM Na-Acetate pH 6.5, 0.005% TWEEN 20 and 50 µM PFI-3[8]) were immobilised to a density of 100-5000 Response Units (RU). The reference surface was subsequently deactivated using 1 M ethanolamine. For VCB immobilisation, streptavidin (Sigma Aldrich, prepared at 1 mg/ml in 10 mM sodium acetate coupling buffer, pH 5.0) was immobilised by amine coupling to a density of 3000-5000 RU after which biotinylated VCB complex (0.125 mM in running buffer) was streptavidin-coupled to a density of 100-500 RU. Biotinylated VCB was prepared as previously described[21]. The reference surface was generated by deactivating the EDC/NHS-treated surface with 1 M ethanolamine. All interaction experiments were done at 6°C in running buffer (20 mM TRIS, pH 8.3, 150 mM potassium chloride, 2 mM magnesium chloride, 2 mM TCEP, 0.005% TWEEN 20, 1% dimethyl sulfoxide). For ternary complex measurements, a sensor chip surface with VCB immobilised was used (preparation as described above). Experiments were run in dual-inject mode with 10 µM SMARCA present during the injection and dissociation phase. Sensorgrams from reference surfaces and blank injections were subtracted from the raw data prior to data analysis using Biacore Insight software. Affinity and binding kinetic parameters were determined by global fitting using the 1:1 interaction model with a term for mass-transport included.

Cell culture

Cell lines were typically cultured in flasks (75cm^2) at sub-confluency, regularly checked for mycoplasma, authenticated by STR profiling (Eurofins Genomics) and kept at low passage numbers in humidified incubators at 37°C and 5% CO_2. Cell lines were obtained from The University of Texas Southwestern Medical Center (HCC-364 RRID:CVCL_5134, HCC-515 RRID:CVCL_5136), DSMZ (KYSE-30 RRID:CVCL_1351, Caco-2 RRID:CVCL_0025), JCRB (LU99 RRID:CVCL_3015), Charles River (LXFA 629L RRID:CVCL_D189, LXFA 923L, LXFL 529L RRID:CVCL_D085, LXFL 1121L) and ATCC (all others). The following media were used: RPMI 1640 "ATCC" with Glutamax + 10% FCS + sodium pyruvate + 10mM HEPES + 0.25% glucose (HCC4006 RRID:CVCL_1269, HCC-364, HCT-15 RRID:CVCL_0292, LU99, NCI-H1568 RRID:CVCL_1476, NCI-H23 RRID:CVCL_1547), RPMI-1640 "Anprotec" with glutamine and HEPES (AC-LM-0054) + 10% FCS + 50µg/ml gentamicin (LXFA 629L, LXFA 923L, LXFL 529L, LXFL 1121L), DMEM + 10% FCS (RKO RRID:CVCL_0504, Caco-2), McCoy's + 10% FCS (HCT116 RRID:CVCL_0291), F12-K + 10% FCS (A549 RRID:CVCL_0023), ACL-4 + 5% FCS (NCI-H1355 RRID:CVCL_1464), EMEM with Glutamax + 10% FCS sodium pyruvate (SK-MEL-5 RRID:CVCL_0527, RKO), 1:1 RPMI : F12 Ham's + 10% FCS (KYSE-30), 1:1 MCDB105 + 1.5g/l sodium bicarbonate : M199 + 2.2g/l sodium bicarbonate + 15% FCS (OV-90 RRID:CVCL_3768, TOV-112D RRID:CVCL_3612), DMEM + 10% FCS + sodium pyruvate + NEAA (SK-N-AS RRID:CVCL_1700), RPMI 1640 + 5% FCS (HCC-515), RPMI 1640 + 20% FCS (MP38 RRID:CVCL_4D11). VH298 was purchased from Tocris, MG132 and MLN4294 were purchased from Merck.

Cell line annotation (CRISPR depletion, gene expression and mutation data) was obtained from Novartis' and the Broad and Sanger Institutes' Cancer Dependency Map ("DepMap") and Cancer Cell Line Encyclopedia ("CCLE") projects (https://depmap.org/portal/).

Cell viability assays

500-2,000 cells were seeded in white, clear bottom 96-well plates (Corning or Perkin Elmer) in 180-200µl medium per well. The next day, compounds were added using a digital dispenser and a "T0" sample was measured for reference. Cells were incubated for 144-192 hours and viability (luminescence) was measured using CellTiter Glo or CellTiter Glo 2.0 (Promega) according to manufacturer's instructions after equilibrating cells and reagents at

room temperature and 10-20 min incubation time while shaking. Values were displayed relative to negative controls (DMSO) and curves were fitted using a 4-parametric logistic model.

SMARCA2/4 capillary electrophoresis protein assays

130,000-200,000 cells were seeded in 24-well plates and incubated until settled down or overnight. Compounds were dissolved in DMSO and added to cells in indicated concentrations using a digital dispenser following an optional media change. Cells were incubated for 4 or 18 hours as indicated. For SMARCA2/4 half-life determination, 150,000 or 200,000 cells were seeded in 24-well plates. The next day, 50 µg/ml cycloheximide (Sigma) was added and cells were incubated for 1-24 hours. For SMARCA2/4 re-synthesis measurements, 200,000 cells were seeded in 24-well plates. The next day, 100 nM compound **6** was added for 4 hours to degrade SMARCA2/4, and a sample was taken as baseline for normalisation. To allow re-synthesis, a VHL binder (compound **32**, 25 or 50 µM) was then added for 3 or 24 hours. Medium was removed, cells were washed with PBS and lysed with 80 µl Lysis Buffer (MSD Tris Lysis Buffer (#R60TX-2) + Halt Inhibitor Cocktail (100x) + Benzonase 0.5 µL/ml). Samples were frozen at -80°C and thawed at room temperature before use. Samples were transferred to a V-bottom plate and insoluble debris was pelleted by centrifugation for 5 minutes at maximum speed. The supernatant was transferred to a fresh plate. Master Mix and Ladder were prepared according to manufacturer's instructions for 12-230 kDa Wes Separation Module, 8x25 capillary cartridges, ProteinSimple #SM-W004 with Anti-Rabbit Detection Module for Wes, Peggy Sue or Sally Sue, Protein Simple #DM-001. 4.8 µl lysate were mixed with 1.2 µl Master Mix to achieve a protein concentration of approximately 0.5 µg/µl. Antibodies were diluted in Antibody Diluent II (SMARCA2 Sigma #HPA029981 RRID:AB_10602406 1:25-100, SMARCA4 Cell Signaling #49360 clone D1Q7F RRID:AB_2728743 1:15-120 or Abcam #ab110641 clone EPNCIR111A RRID:AB_10861578 1:60, GAPDH Abcam #ab9485 RRID:AB_307275 1:250). Wes plates were prepared and run according to manufacturer's instructions. Proteins were quantified with accompanying Compass Software. SMARCA2/4 protein levels were normalised to GAPDH. Values were displayed relative to negative controls (DMSO) unless indicated otherwise. Where applicable, curves were fitted using a 4-parametric logistic model.

qPCR

350,000-500,000 cells were seeded in 6-well plates and compounds were added the next day at the indicated concentrations after pre-dilution in medium. Cells were incubated for 18 hours, harvested, and RNA was extracted using the RNeasy Mini Kit (Qiagen) according to manufacturer's instructions. A DNAse digestion step was included. 1 µg RNA was used for cDNA synthesis with the SuperScript VILO cDNA synthesis kit (Invitrogen) according to manufacturer's instructions. TAQMAN qPCR was then performed using the QuantiTect Multiplex PCR kit (Qiagen) with probes for KRT80 (Hs01372365_m1, Applied Biosystems) and human GAPDH as endogenous control (4326317E, VIC/MGB probe, Primer Limited) for normalisation in a duplex assay over 45 cycles with 100 ng cDNA input. Relative mRNA levels were calculated using the ΔΔCt method and displayed relative to the DMSO control. Curves were fitted using a 4-parametric logistic model.

Imaging-based SMARCA2/4 protein assay in RKO cells

1250 cells per well in 60 µl medium were plated in flat bottom, poly-lysin coated 384-well plates (CellCarrier Ultra, Perkin Elmer). The next day, test compounds (10 µl of serial dilutions) and DMSO controls were diluted in DMEM medium such that the final DMSO content was <1%, or were added using an ultrasound dispensing system. 4 wells were reserved for a background measurement. Cells were incubated for 24 hours and then fixed by adding 25 µl

7.4% formaldehyde (0.2% Triton-X-100) in PBS for 15 minutes at room temperature. After aspirating the fixing solution, the cells were washed once with 25 µl PBS. 25 µl of blocking buffer (10% goat serum in PBS) was added and cells were incubated for 30 minutes, then washed once with PBS. Cells were stained with 20 µl of SMARCA2/4 primary antibody solution (Sigma #HPA029981 RRID:AB_10602406 1:1000 or Cell Signaling #52251 clone E9O6 RRID:AB_2799410 1:1000 in PBS with 10% FCS) for 2-4 hours at room temperature. Cells were again washed once with PBS. 25 µl 5 µg/ml Hoechst 33342 (1:2000, Invitrogen H1399) was added for detection of nuclei, together with Alexa Fluor 647 goat anti mouse IgG (Invitrogen #A32728 RRID:AB_2633277 1:1000) or Alexa Fluor 488 goat anti rabbit IgG (Invitrogen #A11034 RRID:AB_25762171:1000) in PBS with 10% FCS, and cells were incubated for 60 minutes at room temperature. The cell layer was then washed once with 25 µl PBS, the wells were filled with 25 µl PBS and the plates were sealed with an adhesive sheet. They were then imaged on the Opera Phoenix (mean intensity in the nucleus). Results were computed as percent of controls ((value of test compound – background) / (value of the negative control DMSO – background) multiplied by 100). IC_{50} values were computed using a 4-parametric logistic model.

Pharmacokinetic analyses

Compound concentrations in plasma aliquots were measured by quantitative HPLC-MS/MS using an internal standard. Calibration and quality control samples were prepared using blank plasma from untreated animals. Samples were precipitated with acetonitrile and injected into a HPLC system (Agilent 1200). Separation was performed by gradients of 5 mmol/L ammonium acetate pH 4.0 and acetonitrile with 0.1% formic acid on a 2.1 mm by 50 mm XBridge BEH C18 reversed-phase column with 2.5 µm particles (Waters). The HPLC was interfaced by ESI operated in positive ionization mode to a triple quadrupole mass spectrometer (5000 or 6500+ Triple Quad System, SCIEX) operated in multiple reaction monitoring mode. Transitions were 532.4 to 432.8 m/z for BI01810284, 525.6 to 425.7 m/z for BI01802983 and 1021.6 to 624.2 m/z for BI01580883. Chromatograms were analyzed with Analyst (SCIEX) and pharmacokinetic parameters were calculated by non-compartmental analysis using BI-proprietary software.

Solubility testing

Compound solubility was determined by dilution of a 10 mmol/l compound solution in DMSO into buffer to a final concentration of 125 µg/ml. Dilution into a 1:1 mixture of acetonitrile and water was used as reference. After 24 h, the incubations were filtrated and the filtrate was analyzed by LC-UV.

Microsomal stability

The degradation kinetics of 1 µmol/l compound in 0.5 mg/ml liver microsomes were inferred in 100 mM Tris-HCl pH 7.5, 6.5 mM $MgCl_2$ and 1 mM NADPH at 37°C. Reactions were terminated by addition of acetonitrile and precipitates separated by centrifugation. Compound concentrations in supernatants were measured by HPLC-MS/MS and clearance was calculated from compound half-lives using the well-stirred liver model.

Plasma protein binding

Binding of compound to plasma proteins was determined by equilibrium dialysis of 3 µmol/L compound in plasma (or plasma dilutions in PBS) against PBS through an 8 kDa molecular-weight cut-off cellulose membrane (RED device, Thermo Fisher) at 37°C for 5 h. After incubation, aliquots from donor and acceptor compartments were precipitated and the concentrations in the supernatants were determined by quantitative LC-MS/MS. Calibration and quality control samples were prepared using blank plasma and internal standard. The fraction unbound was calculated as ratio of the compound concentration in the acceptor compartment to the concentration in the donor compartment.

Bidirectional permeability measurement in Caco-2 cells

Bidirectional permeability of test compounds across a Caco-2 cell monolayer was measured as described[35] with a modification of preincubation time[36]. Briefly, Caco-2 cells were seeded onto Transwell inserts (#3379, Corning, Wiesbaden, Germany) and cultured for 14–21 days. Cells were incubated with culture media containing 1 µM test compound for 24 hours. After the preincubation period, culture media were removed and fresh transport buffer (128.13 mM NaCl, 5.36 mM KCl, 1 mM $MgSO_4$, 1.8 mM $CaCl_2$, 4.17 mM $NaHCO_3$, 1.19 mM Na_2HPO_4, 0.41 mM NaH_2PO_4, 15 mM 2-[4-(2-hydroxyethyl)piperazin-1-yl]ethanesulfonic acid (HEPES), 20 mM glucose, pH 7.4, 0.25% bovine serum albumin) containing 1 µM test compound was added to the apical (apical to basal) or basal (basal to apical) compartment (donor compartment), transport buffer without test compound was added to the opposite compartment (receiver compartment). Samples were taken at different time points for up to 2 hours. Test compound in the samples was quantified with LC-MS/MS. In order to elucidate the role of drug transporter P-gp in the transcellular transport, permeability measurement was performed in the absence and presence of the selective P-gp inhibitor zosuquidar[36]. Apparent permeability coefficients (Papp,AB, Papp,BA) were calculated as follows:

$$Papp,AB=Q\_AB/((C0\times s\times t)) \quad (1)$$

$$Papp,BA=Q\_BA/((C0\times s\times t)) \quad (2)$$

where Q is the amount of compound recovered in the receiver compartment after the incubation time t, C0 the initial compound concentration given to the donor compartment, and s the surface area of the Transwell inserts. Efflux ratio is calculated as the quotient of Papp,BA (mean of duplicate) to Papp,AB (mean of duplicate). The P-gp substrate apafant and one low permeable compound (BI internal reference, Papp ≈ 3×10^{-7} cm/s, no efflux) were included in every assay plate. In addition, Transepithelial electrical resistance (TEER) values were measured for each plate before the permeability assay. All three parameters (efflux of the reference substrates, Papp values of the low permeable compound, and TEER values) were used to ensure the quality of the assays.

Animals and xenograft experiments

Female BomTac:NMRI-*Foxn1*^{nu} mice were obtained from Taconic Denmark at an age of 6-8 weeks. After arrival of the local animal facility at Boehringer Ingelheim RCV GmbH & Co KG mice were allowed to adjust to housing conditions at least for 5 days before the start of the experiment. Mice were group-housed under pathogen-free and controlled environmental conditions and handled according to the institutional, governmental and European Union guidelines (Austrian Animal Protection Laws, GV-SOLAS and FELASA guidelines). Animal studies were approved by the internal ethics committee and the local governmental committee. Food and water were provided ad libitum. To establish subcutaneous tumours mice were injected with 5 x 10^6 NCI-H1568 in PBS with 5% FCS or with 1 x 10^7 A549 cells in PBS with 5% FCS. Tumour diameters were measured with a caliper three times a week.

The volume of each tumour (in mm^3) was calculated according to the formula "tumour volume = length * diameter^2 * π/6." To monitor side effects of treatment, mice were inspected daily for abnormalities and body weight was determined daily after the start of treatment. Animals were sacrificed when the tumours reached a size of 1,500 mm^3. Mice were randomised into treatment groups when the average tumour size reached ~210-220 mm^3. All administrations were dosed with 10 ml/kg (s.c. and oral). Control mice were dosed subcutaneously with 10% HP-β-CD in 50% Ringer solution and orally with 15% HP-β-CD, that means the control mouse treatment was corresponding to the solvent of the compounds. Compound **6** was dosed subcutaneously either in a d1-4 q3d, d6-8 q2d, d11-13 q2d treatment ("Treatment 1") or a q3 or 4d treatment ("Treatment 2"). Compound **10** was dosed at 30 or 100 mg/kg and ACBI2 at 80 mg/kg, both compounds orally with a daily dosing.

For the evaluation of the statistical significance of tumour growth inhibition, a one-tailed nonparametric Mann-Whitney-Wilcoxon U-test was performed, based on the hypothesis that an effect would only be measurable in one direction (i. e. expectation of tumour inhibition but not tumour stimulation). Analysis was performed on the day indicated for each experiment. The p-values obtained from the U-test were adjusted using the Bonferroni-Holm correction. By convention, p-values ≤0.05 indicate significance of differences.

Immunohistochemistry and imaging analysis

Xenograft samples were fixed in 10% formaldehyde for 24 hours and later moved to ethanol and embedded in paraffin. 2 µm-thick sections were cut using a microtome, then placed on glass slides (KLINIPATH, silan printer slides PR-S:001), and subsequently dewaxed. SMARCA2 immunohistochemistry was carried out on the Leica BOND RX platform (Leica Biosystems) according to manufacturer's instructions using a human-specific SMARCA2 antibody (Cell Signaling #11966 clone D9E8B RRID:AB_2797783 1:400) in a 20 minute incubation in EDTA-based pH 9 ER2 buffer (high-pH epitope retrieval buffer or heat-induced epitope retrieval buffer). After staining, the slides were cover-slipped with Shandon Consul-Mount glass covers, scanned using 3D Histotech slide scanner (Leica Biosystems). All slides were reviewed and evaluated for quality by a board-certified MD specialist in Anatomic Pathology (PC). Imaging analysis was performed using the digital pathology platform HALO (Indica Labs). A tissue-classifying algorithm was trained to selectively recognise viable tumour tissue against stroma, necrosis, and skin. The tissue classification output for each scan was reviewed and manually edited as necessary. A cell detection and scoring algorithm was trained to measure DAB optical density (OD) in the nuclei of tumour cells. A positivity threshold for DAB OD was determined by normalisation with respect to the DAB OD as calculated from *bona fide* negative tissue (e. g., murine stroma as background). The average, background-normalised DAB OD of tumour cell nuclei was used to quantitate SMARCA2 expression in each xenograft sample.

***Ex vivo* human whole blood assay**

The assay was performed on human whole blood from three healthy donors. Aliquots of whole blood were treated in triplicate with a gradient of ACBI2 (starting at 1 µM and six 1:3 dilutions). Samples were pivoted at room temperature for 18 hours in the dark. Subsequently, peripheral blood mononucleated cells (PBMCs) were isolated from individual aliquots using SepMate Tubes (StemCell) and Lymphoprep (StemCell) medium according to the manufacturer's instructions and protein lysates were prepared using MSD Lysis buffer (Mesocale Discovery) supplemented with 1:100 Halt Phosphatase-Protease Inhibitor Cocktail (Thermo Fisher), 0.5 µl/ml benzonase (Novagen) and 10 mM DTT. SMARCA2 and SMARCA4 protein levels were determined using an automated Western blotting system (Bio-Techne) according to manufacturer's instructions. Incubation with primary antibodies for SMARCA2 (Cell Signaling #11966 clone D9E8B RRID:AB_2797783 1:25), SMARCA4 (Abcam #ab110641 clone EPNCIR111A RRID:AB_10861578 1:25) and GAPDH (Abcam, #ab9485 RRID:AB_307275 1:1000) were performed for 30 minutes.

Proteomics

Cells were seeded at 5×10^6 cells on a 100 mm plate 24 hours before treatment. Cells were treated in triplicate by addition of test compounds at 100 nM. After 4 h, the cells were washed twice with 10 ml cold PBS and lysed in 500 µL of 100 mM TEAB with 5% (w/v) SDS. The lysate was pulse sonicated briefly and then centrifuged at 15,000 × *g* for 10 min. Samples were quantified using a micro BCA protein assay kit (Thermo Fisher Scientific). 300 µg of each sample was reduced with DTT, alkalised with iodoacetamide and double-digested with trypsin using the modified S-TRAP mini (ProtiFi) protocol. Peptide quantification was done using Pierce™ Quantitative Fluorometric Peptide Assay and equal amount from each sample was labelled using TMTpro™ 16plex Label Reagent Set (Thermo Fisher Scientific) as per the manufacturer's instructions. The samples were then pooled and desalted using a 7 mm, 3 mL C18 SPE cartridge column (Empore, 3M). The pooled and desalted sample was fractionated using high pH reverse-phase chromatography on an XBridge peptide BEH column (130 Å, 3.5 µm, 2.1 × 150 mm, Waters) on an Ultimate 3000 HPLC system (Thermo Scientific/Dionex). Buffers A (10 mM ammonium formate in water, pH 9) and B (10 mM ammonium formate in 90% acetonitrile, pH 9) were used over a linear gradient of 2% to 100% buffer B over 80 min at a flow rate of 200 µL/min. 80 fractions were collected using a WPS-3000 FC auto-sampler (Thermo Scientific) before concatenation into 20 fractions based on the UV signal of each fraction. All the fractions were dried in a Genevac EZ-2 concentrator and resuspended in 1% formic acid for MS analysis. The fractions were analysed sequentially on a Q Exactive HF Hybrid Quadrupole-Orbitrap Mass Spectrometer (Thermo Scientific) coupled to an Dionex Ultimate 3000 RS (Thermo Scientific). Buffers A (0.1% formic acid in water) and B (0.1% formic acid in 80% acetonitrile) were used over a linear gradient from 5% to 35% buffer B over 125 min and then from 35% buffer B to 98% buffer B in 2 min at a constant flow rate of 300 nl/min. The column temperature was 50 °C. The mass spectrometer was operated in data dependent mode with a single MS survey scan from 335-1600 *m/z* followed by 15 sequential *m/z* dependent MS2 scans. The 15 most intense precursor ions were sequentially fragmented by higher energy collision dissociation (HCD). The MS1 isolation window was set to 0.7 *m/z* and the resolution set at 120,000. MS2 resolution was set at 60,000. The AGC targets for MS1 and MS2 were set at $3x10^6$ ions and $1x10^5$ ions, respectively. The normalised collision energy was set at 32%. The maximum ion injection times for MS1 and MS2 were set at 50 ms and 200 ms respectively. The mass accuracy was checked before the initiation of sample analysis. The raw MS data files for all 20 fractions were merged and searched against the Uniprot-sprot-Human-Canonical database by Maxquant software 2.0.3.0 for protein identification and TMT reporter ion quantitation. The Maxquant parameters were set as follows: enzyme used Trypsin/P; maximum number of missed cleavages equal to two; precursor mass tolerance equal to 10 p.p.m.; fragment mass tolerance equal to 20 p.p.m.; variable modifications: oxidation (M), dioxidation (MW), acetyl (N-term), deamidation (NQ), Gln -> pyro-Glu (Q N-term); fixed modifications: carbamidomethyl (C). The data was filtered by applying a 1% false discovery rate followed by exclusion of proteins with less than two unique peptides. Quantified proteins were filtered if the absolute fold-change difference between the three DMSO replicates was ≥ 1.5.

Western Blot

Cells were seeded into 6-well plates 24 hours before treatment. Next day, several wells were treated with compounds or DMSO as indicated, washed with PBS and lysed with lysis buffer (1% Triton X-100, 150 mM NaCl, 1 mM EDTA, 50 mM Tris pH 7.4, protease inhibitor cocktail (Roche), 50 units/mL benzonase nuclease (Sigma)). Lysates were cleared by centrifugation at 4 °C, at 15800 × *g* for 10 min and the supernatants stored at -20 °C. Protein concentration was determined by BCA assay (Pierce) and the absorbance at 562 nm measured by spectrophotometry (NanoDrop ND1000). Samples were separated by SDS-PAGE using 20 µg of protein per well of NuPAGE Novex 4-12% BIS-TRIS gels (Invitrogen) and transferred to 0.2 µm pore nitrocellulose membrane (Amersham) by wet transfer. Western blot images were obtained through detection of SMARCA2 (Sigma

#HPA029981 RRID:AB_10602406 1:1000), SMARCA4 (Abcam #ab108318 clone EPR3912 RRID:AB_10889900 1:1000), PBRM1 (Bethyl Laboratories #A301-591A RRID:AB_1078808 1:1000), β-actin (Cell Signaling #4970 clone 13E5 RRID:AB_2223172 1:2500) and GAPDH (Abcam #ab9485 RRID:AB_307275 1:2500) antibodies with IRDye 800CW donkey anti-rabbit secondary antibody (LI-COR #926-32213 RRID:AB_621848 1:10000) using a ChemiDoc MP imaging system (Bio-Rad). Western blots were quantified using Image Studio Lite (Licor, version 5.2) with normalisation to loading control and DMSO and further analysed using GraphPad Prism (version 9.2.0).

Molecular Dynamics Simulations

1 µs accelerated molecular dynamics (aMD) simulations were performed in AMBER [37] to exhaustively sample the conformational space of PROTACs compound **10** and ACBI2 in explicit aqueous solution in analogy to earlier established protocols for sampling of peptidic macrocycles[38]. Reweighted conformational ensembles were used to calculate the potential of mean force along the molecular descriptors radius of gyration as a measure of compactness as well as polar surface area to characterise exposed polar regions. Trajectory slicing into five splits of 200 ns demonstrated coverage of conformational space and yielded standard deviations for free energy profiles.

Data Availability

Data generated during the study will be available in a public repository upon publication with the accession codes referenced at mention of dataset, are included in the paper and/or its supplementary information files or available from the corresponding authors upon reasonable request.

Author contributions

C.K. and N.T. designed and synthesised PROTACs, designed and supervised experiments, compiled and analysed data, prepared figures and co-wrote the manuscript. B.M. designed and supervised experiments, compiled and analysed data, prepared figures and co-wrote the manuscript. S.W. co-conceived the study and designed, supervised and analysed experiments. M.W. conceived and supervised *in vivo* work, analysed xenograft experiments and contributed text to the manuscript. N.M. and J.R. designed and supervised *in vivo* PK experiments and *in vitro* ADME assays. M.R. designed and carried out protein crystallography experiments, interpreted, compiled and deposited structural data, prepared figures and contributed text to the manuscript. G.B. designed and supervised protein crystallography experiments, interpreted, compiled and deposited structural data, prepared figures and contributed text to the manuscript. P.G. and G.Ga. characterised, optimised and scaled up synthesis of compounds and contributed text to the manuscript. E.D. designed and synthesised PROTACs. R.M. optimised new methods for the synthesis of PROTACs. C.W. and V.V. designed and performed cellular experiments. V.V. performed unbiased whole cell proteomics assays. K.R. designed and supervised SPR experiments. M.S. developed SPR assays and acquired and evaluated data. J.E.F. performed enhanced sampling simulations. T.G. Designed and supervised cooperativity and ternary complex affinity TR-FRET experiments. Y.C. designed, supervised, and analysed permeability measurements. G.Gr. designed and coordinated biomarker analyses and contributed text to the manuscript. P.C. coordinated and analysed immunohistochemistry experiments. S.H. set up and analysed ex vivo human whole blood assays. N.B. optimised and performed immunohistochemistry experiments. G.Gm. and M.M. designed, performed and analysed NOE experiments, compiled and documented analytical data and contributed text to the manuscript. M.K. co-conceived the study, co-wrote the manuscript and designed, supervised and analysed experiments. A.C. co-conceived the study, designed and supervised experiments and edited the manuscript. H.W. co-conceived the study, designed PROTACs, prepared figures and co-wrote the manuscript. W.F. co-conceived the study, designed PROTACs, designed, supervised and analysed experiments, prepared figures and co-wrote the manuscript.

Competing interests

The authors declare the following competing financial interest(s): The Ciulli laboratory receives or has received sponsored research support from Almirall, Amphista therapeutics, Boehringer Ingelheim, Eisai, Nurix therapeutics and Ono Pharmaceuticals. A.C. is a scientific founder, shareholder and consultant of Amphista therapeutics, a company that is developing targeted protein degradation therapeutic platforms. C.K., B.M., S.W., M.W., N.M., G.B., P.G., G.Ga., K.R., M.S., J.E.F., T.G., Y.C., G.Gr., P.C., S.H., N.B., J.R., G.Gm., M.M., M.K. and H.W. are current or former employees of Boehringer Ingelheim. S.W. is now an employee of Merck; E.D. is now an employee of Astra Zeneca. This work has received funding from Boehringer Ingelheim. Biophysics and drug discovery activities at Dundee were supported by Wellcome Trust strategic awards to Dundee (100476/Z/12/Z and 094090/Z/10/Z, respectively). The Austrian Promotion Agency has funded the project from 2018 until 2021 with the frontrunner grant number 871904 within the general program.

Acknowledgements

The authors would like to thank Erich Spielvogel, Patrick Werni, Teresa Gmaschitz, Karin-Stefanie Hofbauer, Martina Kohla, Oliver Petermann, Johannes Wachter, Carina Riedmüller, Daniel Zach, Sabine Kallenda, Janine Rippka, Markus Graf-Gabriel, Teresa Puchner, Sonja Porits, Katrin Gitschtaler, Andreas Schrenk, Renate Schnitzer, Bernhard Wolkerstorfer and Niklas Baumann (all Boehringer Ingelheim) and Abdel Atrih and Douglas Lamont (both Dundee FingerPrints Proteomics facility) for technical and experimental support, and Mark Pearson, Darryl McConnell and Mark Petronczki (all Boehringer Ingelheim) for critical feedback. We also thank the Diamond Light Source for beamtime (BAG proposal MX14980) and for beamline support at beamline and I24.

Supplementary Information is available for this paper.

Correspondence and requests for materials should be addressed Harald Weinstabl or William Farnaby (harald.weinstabl@boehringer-ingelheim.com, w.farnaby@dundee.ac.uk).

References

1. Farnaby, W., Koegl, M., McConnell, D. B. & Ciulli, A. Transforming targeted cancer therapy with PROTACs: A forward-looking perspective. *Curr Opin Pharmacol* 57, 175–183 (2021).

2. Alabi, S. & Crews, C. Major Advances in Targeted Protein Degradation: PROTACs, LYTACs, and MADTACs. *J Biol Chem* 100647 (2021) doi:10.1016/j.jbc.2021.100647.

3. Sun, X. *et al.* Protacs: Great opportunities for academia and industry. *Signal Transduct Target Ther* 4, 64 (2019).

4. Garber, K. The PROTAC gold rush. *Nat Biotechnol* 40, 12–16 (2022).

5. Oike, T. *et al.* A synthetic lethality-based strategy to treat cancers harboring a genetic deficiency in the chromatin remodeling factor BRG1. *Cancer Res* 73, 5508–18 (2013).

6. Wilson, B. G. *et al.* Residual complexes containing SMARCA2 (BRM) underlie the oncogenic drive of SMARCA4 (BRG1) mutation. *Mol Cell Biol* 34, 1136–44 (2014).

7. Hoffman, G. R. *et al.* Functional epigenetics approach identifies BRM/SMARCA2 as a critical synthetic lethal target in BRG1-deficient cancers. *Proc. Natl. Acad. Sci. U. S. A* 111, 3128–3133 (2014).

8. Gerstenberger, B. S. *et al.* Identification of a Chemical Probe for Family VIII Bromodomains through Optimization of a Fragment Hit. *J Med Chem* 59, 4800–4811 (2016).

9. Albrecht, B. K. *et al.* Therapeutic pyridazine compounds and uses thereof. (2016).

10. Farnaby, W. *et al.* BAF complex vulnerabilities in cancer demonstrated via structure-based PROTAC design. *Nat Chem Biol* 15, 672–680 (2019).

11. Alqahtani, M. S., Kazi, M., Alsenaidy, M. A. & Ahmad, M. Z. Advances in Oral Drug Delivery. *Front Pharmacol* 12, 618411 (2021).

12. Sutherell, C. L. *et al.* Identification and Development of 2,3-Dihydropyrrolo[1,2-a]quinazolin-5(1H)-one Inhibitors Targeting Bromodomains within the Switch/Sucrose Nonfermenting Complex. *J Med Chem* 59, 5095–5101 (2016).

13. Roy, M. J. *et al.* SPR-Measured Dissociation Kinetics of PROTAC Ternary Complexes Influence Target Degradation Rate. *Acs Chem Biol* 14, 361–368 (2019).

14. Atilaw, Y. *et al.* Solution Conformations Shed Light on PROTAC Cell Permeability. *Acs Med Chem Lett* 12, 107–114 (2020).

15. Weerakoon, D., Carbajo, R. J., Maria, L. D., Tyrchan, C. & Zhao, H. Impact of PROTAC Linker Plasticity on the Solution Conformations and Dissociation of the Ternary Complex. *J Chem Inf Model* (2021) doi:10.1021/acs.jcim.1c01036.

16. Xiang, W. *et al.* Discovery of ARD-2585 as an Exceptionally Potent and Orally Active PROTAC Degrader of Androgen Receptor for the Treatment of Advanced Prostate Cancer. *J Med Chem* 64, 13487–13509 (2021).

17. Mullard, A. Targeted protein degraders crowd into the clinic. *Nat Rev Drug Discov* 20, 247–250 (2021).

18. Snyder, L. B. *et al.* Abstract 43: Discovery of ARV-110, a first in class androgen receptor degrading PROTAC for the treatment of men with metastatic castration resistant prostate cancer. *Exp Mol Ther* 43–43 (2021) doi:10.1158/1538-7445.am2021-43.

19. Pike, A., Williamson, B., Harlfinger, S., Martin, S. & McGinnity, D. F. Optimising proteolysis-targeting chimeras (PROTACs) for oral drug delivery: a drug metabolism and pharmacokinetics perspective. *Drug Discov Today* 25, 1793–1800 (2020).

20. Papillon, J. P. N. *et al.* Discovery of Orally Active Inhibitors of Brahma Homolog (BRM)/SMARCA2 ATPase Activity for the Treatment of Brahma Related Gene 1 (BRG1)/SMARCA4-Mutant Cancers. *J Med Chem* 61, 10155–10172 (2018).

21. Gadd, M. S. *et al.* Structural basis of PROTAC cooperative recognition for selective protein degradation. *Nat Chem Biol* 13, 514–521 (2017).

22. Smith, B. E. *et al.* Differential PROTAC substrate specificity dictated by orientation of recruited E3 ligase. *Nat Commun* 10, 131 (2019).

23. Pierre, R. S. & Kadoch, C. Mammalian SWI/SNF complexes in cancer: emerging therapeutic opportunities. *Curr Opin Genet Dev* 42, 56–67 (2017).

24. Chabanon, R. M., Morel, D. & Postel-Vinay, S. Exploiting epigenetic vulnerabilities in solid tumors: novel therapeutic opportunities in the treatment of SWI/SNF-defective cancers. *Semin Cancer Biol* 61, 180–198 (2019).

25. Xiao, L. *et al.* Targeting SWI/SNF ATPases in enhancer-addicted prostate cancer. *Nature* 1–6 (2021) doi:10.1038/s41586-021-04246-z.

26. Kabsch, W. XDS. *Acta Crystallogr Sect D Biological Crystallogr* 66, 125–132 (2010).

27. McCoy, A. J. *et al.* Phaser crystallographic software. *J Appl Crystallogr* 40, 658–674 (2007).

28. Project, N. 4 C. C. The CCP4 suite: programs for protein crystallography. *Acta Crystallogr Sect D Biological Crystallogr* 50, 760–763 (1994).

29. Emsley, P., Lohkamp, B., Scott, W. G. & Cowtan, K. Features and development of Coot. *Acta Crystallogr Sect D Biological Crystallogr* 66, 486–501 (2010).

30. Chen, V. B. *et al.* MolProbity: all-atom structure validation for macromolecular crystallography. *Acta Crystallogr Sect D Biological Crystallogr* 66, 12–21 (2010).

31. Krissinel, E. & Henrick, K. Inference of Macromolecular Assemblies from Crystalline State. *J Mol Biol* 372, 774–797 (2007).

32. Vonrhein, C. *et al.* Data processing and analysis with the autoPROC toolbox. *Acta Crystallogr Sect D Biological Crystallogr* 67, 293–302 (2011).

33. Vonrhein, C. *et al.* Advances in automated data analysis and processing within autoPROC , combined with improved characterisation, mitigation and visualisation of the anisotropy of diffraction limits using STARANISO. *Acta Crystallogr Sect Found Adv* 74, a360–a360 (2018).

34. Smart, O. S. *et al.* Exploiting structure similarity in refinement: automated NCS and target-structure restraints in BUSTER. *Acta Crystallogr Sect D Biological Crystallogr* 68, 368–380 (2012).

35. Sieger, P., Cui, Y. & Scheuerer, S. pH-dependent solubility and permeability profiles: A useful tool for prediction of oral bioavailability. *Eur J Pharm Sci* 105, 82–90 (2017).

36. Cui, Y. *et al.* A Bidirectional Permeability Assay for beyond Rule of 5 Compounds. *Pharm* 13, 1146 (2021).

37. Salomon-Ferrer, R., Case, D. A. & Walker, R. C. An overview of the Amber biomolecular simulation package. *Wiley Interdiscip Rev Comput Mol Sci* 3, 198–210 (2013).

38. Kamenik, A. S., Lessel, U., Fuchs, J. E., Fox, T. & Liedl, K. R. Peptidic Macrocycles - Conformational Sampling and Thermodynamic Characterization. *J Chem Inf Model* 58, 982–992 (2018).